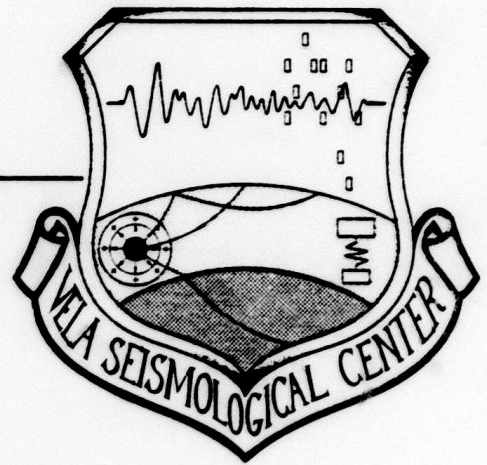


AD A114879

VSC-TR-82-19

A DISCRIMINATION ANALYSIS
OF REGIONAL SEISMIC DATA
RECORDED AT TONTO FOREST
OBSERVATORY FROM NEVADA
TEST SITE EXPLOSIONS AND
NEARBY EARTHQUAKES



J. R. Murphy
T. J. Bennett
T. K. Tzeng

SYSTEMS, SCIENCE AND SOFTWARE
P. O. Box 1620
La Jolla, California 92038

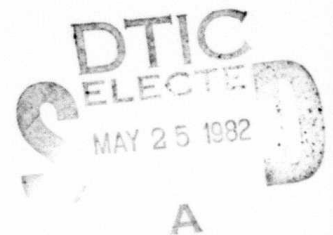
SEMIANNUAL TECHNICAL REPORT, PART I

December 1981

Approved for Public Release,
Unlimited Distribution.

Monitored by:

VELA Seismological Center
312 Montgomery Street
Alexandria, Virginia 22314



DTIC FILE COPY

82 05 25 010

AFTAC Project Authorization No. VT/0701/B/PMP

ARPA Order No. 2551, Program Code No. 6H189

Effective Date of Contract: 1 April 1981

Contract Expiration Date: 30 September 1982

Amount of Contract: \$1,004,347.00

Contract No. F8606-80-C-0016

Principal Investigators and Phone Nos.

Dr. John M. Savino, (714) 453-0060, Ext. 453

Mr. John R. Murphy, (703) 476-5197

Project Scientist and Phone No.

Mr. Brian W. Barker, (202) 325-7581

This research was supported by the Advanced Research Projects Agency of the Department of Defense and was monitored by AFTAC/VSC, Patrick Air Force Base, Florida, 32925, under Contract No. F08606-80-C-0016.

The views and conclusions contained in this document are those of the authors and should not be interpreted as necessarily representing the official policies, either expressed or implied, of the Advanced Research Projects Agency, the Air Force Technical Applications Center, or the U. S. Government.

S³ Project No. 11143

UNCLASSIFIED

SECURITY CLASSIFICATION OF THIS PAGE (When Data Entered)

REPORT DOCUMENTATION PAGE		READ INSTRUCTIONS BEFORE COMPLETING FORM
1. REPORT NUMBER VSC-TR-82-19	2. GOVT ACCESSION NO. AD-A114879	3. RECIPIENT'S CATALOG NUMBER
4. TITLE (and Subtitle) A DISCRIMINATION ANALYSIS OF REGIONAL SEISMIC DATA RECORDED AT TONTO FOREST OBSERVATORY FROM NEVADA TEST SITE EXPLOSIONS AND NEARBY EARTHQUAKES		5. TYPE OF REPORT & PERIOD COVERED Semiannual, April, 1981-October, 1981
		6. PERFORMING ORG. REPORT NUMBER SSS-R-82-5301
7. AUTHOR(s) J. R. Murphy T. J. Bennett T. K. Tzeng		8. CONTRACT OR GRANT NUMBER(s) F08606-80-C-0016
		10. PROGRAM ELEMENT, PROJECT, TASK AREA & WORK UNIT NUMBERS Program Code No. 6H189 ARPA Order No. 2551
9. PERFORMING ORGANIZATION NAME AND ADDRESS Systems, Science and Software P. O. Box 1620 La Jolla, California 92038		12. REPORT DATE December 1981
11. CONTROLLING OFFICE NAME AND ADDRESS VELA Seismological Center 312 Montgomery Street Alexandria, Virginia 22314		13. NUMBER OF PAGES 63
14. MONITORING AGENCY NAME & ADDRESS (if different from Controlling Office)		15. SECURITY CLASS. (of this report) Unclassified
		15a. DECLASSIFICATION/DOWNGRADING SCHEDULE
16. DISTRIBUTION STATEMENT (of this Report) Approved for Public Release, Unlimited Distribution.		
17. DISTRIBUTION STATEMENT (of the abstract entered in Block 20, if different from Report)		
18. SUPPLEMENTARY NOTES		
19. KEY WORDS (Continue on reverse side if necessary and identify by block number) Regional Discrimination NTS Explosions Regional Seismic Phases Long-period Rayleigh Waves Spectral Discriminant M _s versus m _b		
20. ABSTRACT (Continue on reverse side if necessary and identify by block number) The principal objectives of the research reported here are to identify any diagnostic differences between regional seismic phases produced by earthquakes and underground nuclear explosions and to assess their applicability to events occurring in various regions of the U.S.S.R. Two approaches are used: one employs traditional time-domain amplitude and period measurements to compare the relative excitation of various regional phases for earthquakes and explosions,		

DD FORM 1 JAN 73 1473

EDITION OF 1 NOV 68 IS OBSOLETE

UNCLASSIFIED

SECURITY CLASSIFICATION OF THIS PAGE (When Data Entered)

ABSTRACT (continued)

while the second focuses on more sophisticated measurement or processing techniques such as spectral ratios or narrow-band filtering to extract information about frequency differences in the signals generated by the two types of events.

The research reported here was directed at identification of discriminants based on measurements of seismic phases at regional distances from a well-controlled set of Western U.S. explosions and nearby earthquakes. The set includes more than 50 Nevada Test Site events (explosions and nearby earthquakes) recorded at the Tonto Forest Observatory in Arizona. The investigation included spectral analyses of the short-period regional phases, P_n , P_g and L_g which follows-up a previously reported study of time-domain characteristics of these phases. In addition, the current study includes an analysis of the time-domain characteristics of the long-period data from the Nevada Test Site event set, with particular emphasis on the potential applicability of the M_s/m_b discriminant to the identification of small events ($m_b < 4.0$) for which teleseismic M_s data are not generally available.

The principal finding of this study is the discovery of a potential discriminant based on frequency differences in the L_g phases generated by earthquakes and explosions. Spectral analyses of the regional phases demonstrate that, while the average spectral shapes of the P_n and P_g phases from the two source types do not show statistically significant differences, the average earthquake L_g phase appears to be significantly richer in high frequency content than the corresponding average explosion L_g phase. On the basis of this observation, a preliminary L_g spectral ratio discriminant has been defined and applied to the available data set to provide almost complete separation of data from the two source types.

In the analysis of the time-domain characteristics of the long-period data it has been found that quite small events ($m_b < 4.0$) produce observable simple, pulse-like long-period Rayleigh waveforms in the near regional distance range. However, a regional analog of the M_s/m_b discriminant provided by comparing the maximum amplitudes of these long-period signals with those from short-period regional phases P_n , P_g and L_g , is only partially successful in discriminating earthquake and explosion source types. Although, the data for the single station measurements from the two source types are separated, on the average, the discrimination does not appear to be particularly reliable for small events with m_b less than about 4.0.

TABLE OF CONTENTS

<u>Section</u>	<u>Page</u>
I. INTRODUCTION.	1
II. SPECTRAL CHARACTERISTICS OF SHORT-PERIOD REGIONAL PHASE DATA	3
III. TIME-DOMAIN MEASUREMENTS OF LONG-PERIOD PHASES AT REGIONAL DISTANCES.	37
IV. SUMMARY AND CONCLUSIONS	57
4.1 SUMMARY.	57
4.2 CONCLUSIONS.	58
REFERENCES.	61

Accession For	
NTIS GRA&I	<input checked="" type="checkbox"/>
DTIC TAB	<input type="checkbox"/>
Unannounced	<input type="checkbox"/>
Justification	
By _____	
Distribution/	
Availability Codes	
Avail and/or	
List	Special
A	



LIST OF ILLUSTRATIONS

<u>Figure</u>	<u>Page</u>
1. Map showing locations of selected earthquake epicenters with respect to NTS and TFO	4
2. Representative sample ($3.7 \leq m_b \leq 4.3$) of vertical-component, short-period seismograms recorded at station TFO from NTS explosions.	8
3. Representative sample ($3.7 \leq m_b \leq 4.3$) of vertical-component, short-period seismograms recorded at station TFO from earthquakes located near NTS	9
4. Comparison of P_n and L_g amplitudes recorded at station TFO from NTS explosions and earthquakes.	11
5. Comparison of vertical-component seismograms recorded at TFO from an explosion and two nearby earthquakes of about the same magnitude.	12
6. Comparison of regional phase spectra observed at TFO from an explosion (Rivet III, left) and an earthquake (3/23/70, right) of about the same magnitude	15
7. Average S/N as a function of frequency for P_n , P_g and L_g phases recorded at TFO from the selected NTS earthquake sample. Dashed lines denote one standard error of estimate in the mean (σ)	16
8. Average S/N as a function of frequency for P_n , P_g and L_g phases recorded at TFO from the selected NTS explosion sample. Dashed lines denote one standard error of estimate in the mean (σ)	17
9. Comparison of average earthquake and explosion P_n spectra ($3.7 \leq m_b \leq 4.3$) derived from NTS events recorded at TFO	19
10. Comparison of average earthquake and explosion P_g spectra ($3.7 \leq m_b \leq 4.3$) derived from NTS events recorded at TFO	20

LIST OF ILLUSTRATIONS (CONT'D)

<u>Figure</u>	<u>Page</u>
11. Comparison of average earthquake and explosion L_g spectra ($3.7 \leq m_b \leq 4.3$) derived from NTS events recorded at TFO	21
12. Comparison of vertical-component L_g spectral ratio discriminant (ratio of average amplitude levels in 0.5 to 1.0 Hz and 2.0 to 4.0 Hz pass-bands) for NTS explosions and earthquakes ($3.7 \leq m_b \leq 4.3$)	23
13. Comparison of vertical-component L_g spectral ratio discriminant (ratio of average amplitude levels in 0.5 to 1.0 Hz and 2.0 to 4.0 Hz pass-bands) for NTS explosions and earthquakes ($3.3 \leq m_b \leq 4.8$)	24
14. Comparison of vertical (Z), radial (R) and tangential (T) component average earthquake and explosion L_g spectra derived from NTS events recorded at TFO.	26
15. Comparison of vertical (Z), radial (R) and tangential (T) component L_g spectral ratio discriminant for NTS explosions and earthquakes	27
16. Comparison of broadband and bandpass filtered ($f_c \approx 6.6$ Hz) time histories computed from data recorded at Tonopah, Nevada ($\Delta \approx 170$ km) from the Massachusetts Mountain earthquake (EO75, 8/5/71) and a nearby NTS explosion (#235) of the same magnitude (Murphy, 1975).	29
17. Comparison of theoretical L_g spectra from a shallow explosion (left) and an earthquake (right) with a focal depth of 4 km	32
18. Comparison of theoretical L_g spectra computed for the same earthquake at focal depths of 4, 7 and 10 km.	34
19. Comparison of theoretical L_g spectra computed for two earthquakes with the same focal depth (4 km) but different focal mechanisms.	35

LIST OF ILLUSTRATIONS (CONT'D)

<u>Figure</u>	<u>Page</u>
20. Long-period Rayleigh wave amplitude versus short-period P_n amplitude for an NTS explosion and earthquake sample recorded at MINA and KANAB (after Peppin and McEvelly, 1974)	39
21. Typical long-period Rayleigh wave signals from NTS explosions and nearby earthquakes recorded at TFO. Vertical bars indicate relative amplitude scale.	43
22. Dominant period of long-period Rayleigh wave pulses observed at TFO for NTS explosions and earthquakes as a function of network average m_b	45
23. Amplitudes of long-period Rayleigh wave pulses observed at TFO for NTS explosions and earthquakes as a function of network average m_b . Slopes of the least-squares trends were constrained to one	47
24. Amplitudes of long-period Rayleigh wave pulses versus short-period P_n for NTS explosions and earthquakes	48
25. Amplitudes of long-period Rayleigh wave pulses versus short-period P_g for NTS explosions and earthquakes	49
26. Amplitudes of long-period Rayleigh wave pulses versus short-period L_g for NTS explosions and earthquakes	50
27. Transmission path crustal model (top left) and source crustal model (top right) used to compute synthetic seismogram (middle) for an NTS explosion recorded on long-period seismograph at TFO as compared with an observed signal (bottom).	53
28. Comparison of observed and predicted long-period Rayleigh wave amplitudes for NTS explosions in various source media. Straight line corresponds to observed amplitude equal to that predicted using standard scaling relations and teleseismic yield estimate.	56

LIST OF TABLES

<u>Table</u>		<u>Page</u>
1.	Earthquake sample	5
2.	Explosion sample	7
3.	Basin and Range Structural Model	31
4.	Explosion sample	41
5.	Earthquake sample	42

I. INTRODUCTION

This report, together with a companion classified document which is currently in preparation, describes the status of an ongoing research investigation into the application of regional seismic phase data to the discrimination of earthquakes and underground nuclear explosions. The principal objectives of this research are to identify any diagnostic differences between the regional phases produced by the two source types and to assess their applicability to events occurring in various regions of the U.S.S.R. The research program includes two distinct approaches. The first employs traditional, time-domain amplitude and period measurements to compare the relative excitation of different regional phases observed from earthquakes and explosions. The second approach focuses on the evaluation of the capabilities of more sophisticated measurement or processing techniques, such as spectral ratios or narrow-band filtering, in the discrimination analysis of regional phase data. Most of the research previously reported under this contract (Bennett et al., 1981) has been concentrated on the time domain analysis approach, using the most readily available, short-period analog data. This report extends these earlier studies to include time domain analyses of some long-period regional data as well as a detailed spectral analysis of a sample of data recorded from Western U.S. explosions and nearby earthquakes.

The results of the spectral analysis of short-period regional phase data recorded from Western U.S. explosions and earthquakes are presented in Section II where they are compared with the results of previously conducted time domain analyses of essentially the same data set. The data used in this investigation consist of P_n , P_g and L_g phases from more than 50 Nevada Test Site events (explosions and nearby earthquakes) recorded at the Tonto Forest Observatory in Arizona.

The time domain characteristics of the long-period data recorded from earthquakes and explosions at regional distances are assessed in Section III, with particular emphasis on the potential applicability of the M_s/m_b discriminant to the identification of small events ($m_b < 4.0$) for which teleseismic M_s data are generally not available. This is followed in Section IV by a summary, together with a statement of conclusions regarding the current state of knowledge with respect to these issues.

II. SPECTRAL CHARACTERISTICS OF SHORT-PERIOD REGIONAL PHASE DATA

Investigations of the potential value of regional seismic phases such as P_n , P_g and L_g for purposes of discriminating between underground explosions and earthquakes have been pursued in numerous studies dating back to the beginning of the underground nuclear testing program (e.g. Willis et al., 1963). However, it has often been difficult to provide definitive interpretations of the results of many of these previous studies because of the fact that the epicentral locations of the earthquake and explosive sources used in these studies typically have not coincided very closely. That is, given the well-documented variability of regional phase characteristics with changes in propagation path, it has been difficult to attribute observed differences between the earthquake and explosion populations to characteristic differences in source excitation with any real degree of confidence. Consequently, in the present study, the analysis has focused on a well-controlled data set recorded at the Tonto Forest Observatory (TFO), in Central Arizona from a sample of Nevada Test Site (NTS) explosions and Southern Nevada earthquakes located within about one degree of NTS. The locations of the selected earthquakes with respect to NTS and TFO are shown in Figure 1 where it can be seen that they are tightly clustered around the source area of the explosions at an average range of about 550 km from TFO. The initial sample selected for digital processing consisted of 22 earthquakes in the magnitude range of $3.3 \leq m_b \leq 4.8$. However, it was subsequently found that all of the earthquakes with $m_b > 4.3$ were badly clipped and this, together with other recording problems (timing, etc.) reduced the usable sample to the 14 earthquakes listed in Table 1. It can be seen from this table that of the nine events which have been assigned a significant focal depth

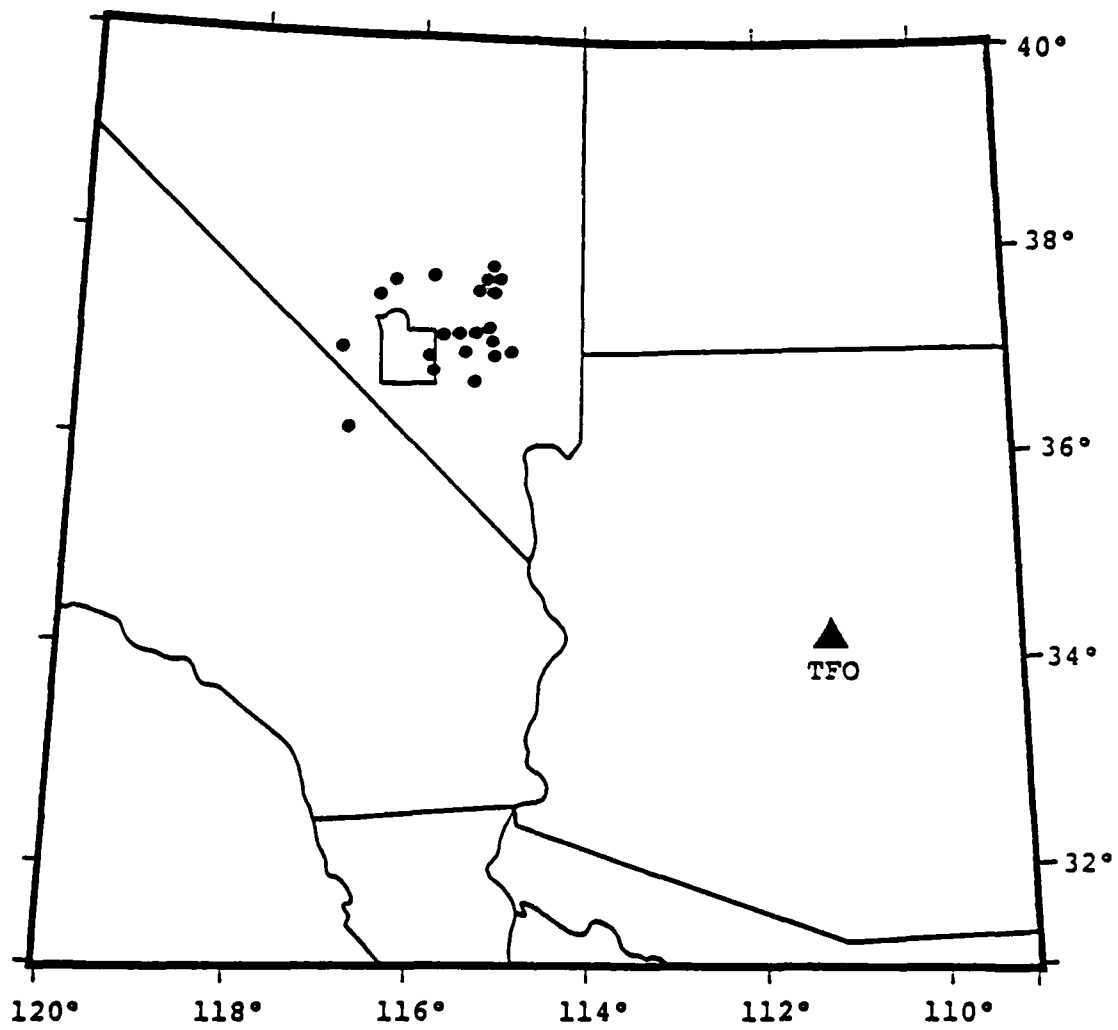


Figure 1. Map showing locations of selected earthquake epicenters with respect to NTS and TFO.

TABLE 1
EARTHQUAKE SAMPLE

<u>Date</u>	<u>Origin Time (UT)</u>	<u>Location</u>		<u>m_b</u>	<u>Focal Depth, km</u>
		<u>Latitude</u>	<u>Longitude</u>		
12/11/67	02:35:21.1	37.20N	115.20W	3.3	33
07/05/74	13:10:29.4	36.17N	116.83W	3.3*	8
01/24/72	13:30:53.9	36.71N	115.47W	3.4*	10
07/30/73	09:18:42.1	37.61N	115.15W	3.5*	5
03/11/68	07:34:24.2	37.00N	115.50W	3.6	33
07/06/71	19:22:39.4	37.49N	116.56W	3.6	5
11/17/65	09:41:28.3	37.60N	115.20W	3.7	33
07/18/63	04:01:16.3	37.20N	115.60W	3.9	25
05/09/67	00:42:25.9	37.00N	115.00W	3.9	33
04/06/66	17:56:32.1	37.20N	115.40W	4.1	33
08/10/70	10:48:56.4	37.19N	115.87W	4.1	3
02/09/73	23:10:34.4	36.84N	115.94W	4.2*	5
03/23/70	19:52:10.7	37.71N	115.99W	4.3	5
08/05/71	17:58:17.1	36.89N	115.97W	4.3	4

* M_L , m_b not available

(i.e. not set to 33 km), eight have focal depths of less than 10 km and, of these, six have been assigned depths of 5 km or less. Thus, the evidence indicates that the selected earthquake sample consists primarily of shallow, upper crustal events. Due to the relatively small size of these events and the absence of an adequate local recording network during the period when most of these events were recorded, focal mechanism solutions are generally not available. However, it is believed that both the Massachusetts Mountain (8/5/71) and Ranger Mountain (2/9/73) earthquakes were predominantly strike-slip events on nearly vertical fault planes (Fisher et al., 1972).

The selected explosion sample consists of 30 Yucca Flat and Rainier Mesa events with body wave magnitudes in the range $3.7 \leq m_b \leq 4.8$. The characteristics of these events are summarized in Table 2 from which it can be seen that these are low yield explosions detonated in alluvium and tuff emplacement media, most of which would be classified as dry. Thus, the selected data sample is well-controlled in the sense that it consists of closely spaced explosions and shallow focus earthquakes covering essentially the same magnitude range.

A representative sample of short-period recordings of NTS explosions at TFO is shown in Figure 2. These are vertical component seismograms arranged in order of increasing body wave magnitude in the range $3.7 \leq m_b \leq 4.3$. As was noted in a previous report (Bennett et al., 1981), the main features of these recordings are weak initial P_n arrivals followed by much larger P_g arrivals which are fairly consistent from event to event. The later arriving L_g phase, although easily identifiable on some of the recordings, is generally less distinct than P_g and shows considerable variability even for these closely spaced explosive events. A corresponding sample of earthquake seismograms covering the same magnitude range is shown in Figure 3. The general characteristics of these

TABLE 2

EXPLOSION SAMPLE

<u>Name</u>	<u>Date</u>	<u>Origin Time (UT)</u>	<u>m_b</u>	<u>Yield,** kt</u>	<u>Source Medium</u>
Petrel	06/11/65	19:45:00.04	3.7*	1.2	Alluvium
Effendi	04/27/67	14:45:00.00	3.8	L	Alluvium
Fawn	04/07/67	15:00:00.04	3.9	L	Alluvium
Mudpack	12/16/64	20:10:00.10	4.0*	2.7	Tuff
Newark	09/29/66	14:45:30.09	4.1	L	Alluvium
Jal	03/19/70	14:03:30.04	4.1	L	Alluvium
Cyclamen	05/05/66	14:00:00.04	4.2	13	Alluvium
Tapestry	05/12/66	19:37:26.20	4.2	L	Alluvium
Rivet III	03/02/67	15:00:00.00	4.2	L	Alluvium
Beebalm	05/01/70	14:13:00.04	4.2	L	Tuff
Plaid II	02/03/66	18:17:37.10	4.3	L	Alluvium
Chocolate	04/21/67	15:09:00.00	4.3	L	Alluvium
Arabis	03/06/70	15:00:00.21	4.3	L	Tuff
Persimmon	02/23/67	18:34:00.04	4.4	L	Alluvium
Zinnia	05/17/72	14:10:00.16	4.4	L	Alluvium
Merlin	02/16/65	17:30:00.04	4.5*	10	Alluvium
Cyathus	03/06/70	14:24:00.94	4.5	L	Tuff
New Point	12/13/66	21:00:00.08	4.6	L	Alluvium
Barsac	03/20/69	18:12:00.04	4.6	L	Alluvium
Fob	01/23/70	16:30:00.21	4.6	L	Tuff
Ajo	01/30/70	17:00:00.04	4.6	L	Alluvium
Diana Mist	02/11/70	19:15:00.04	4.6	L	Tuff
Snubber	04/21/70	14:30:00.04	4.6	L	Tuff
Ildrim	07/16/69	13:02:30.04	4.7	L-I	Tuff
Pliers	08/27/69	13:45:00.04	4.7	L	Alluvium
Labis	02/05/70	15:00:00.04	4.7	L-I	Tuff
Ward	02/08/67	15:15:00.13	4.8	L	Alluvium
Vise	01/30/69	15:00:00.04	4.8	L-I	Alluvium
Lovage	12/17/69	15:15:00.04	4.8	L	Alluvium
Can	04/21/70	15:00:00.04	4.8	L-I	Tuff

* m_b value estimated from the approximate scaling law $m_b = 3.65 + 0.81 \log W$

** Springer and Kinnaman (1971): L denotes 0 to 20 kt, L-I denotes 20 to 200 kt

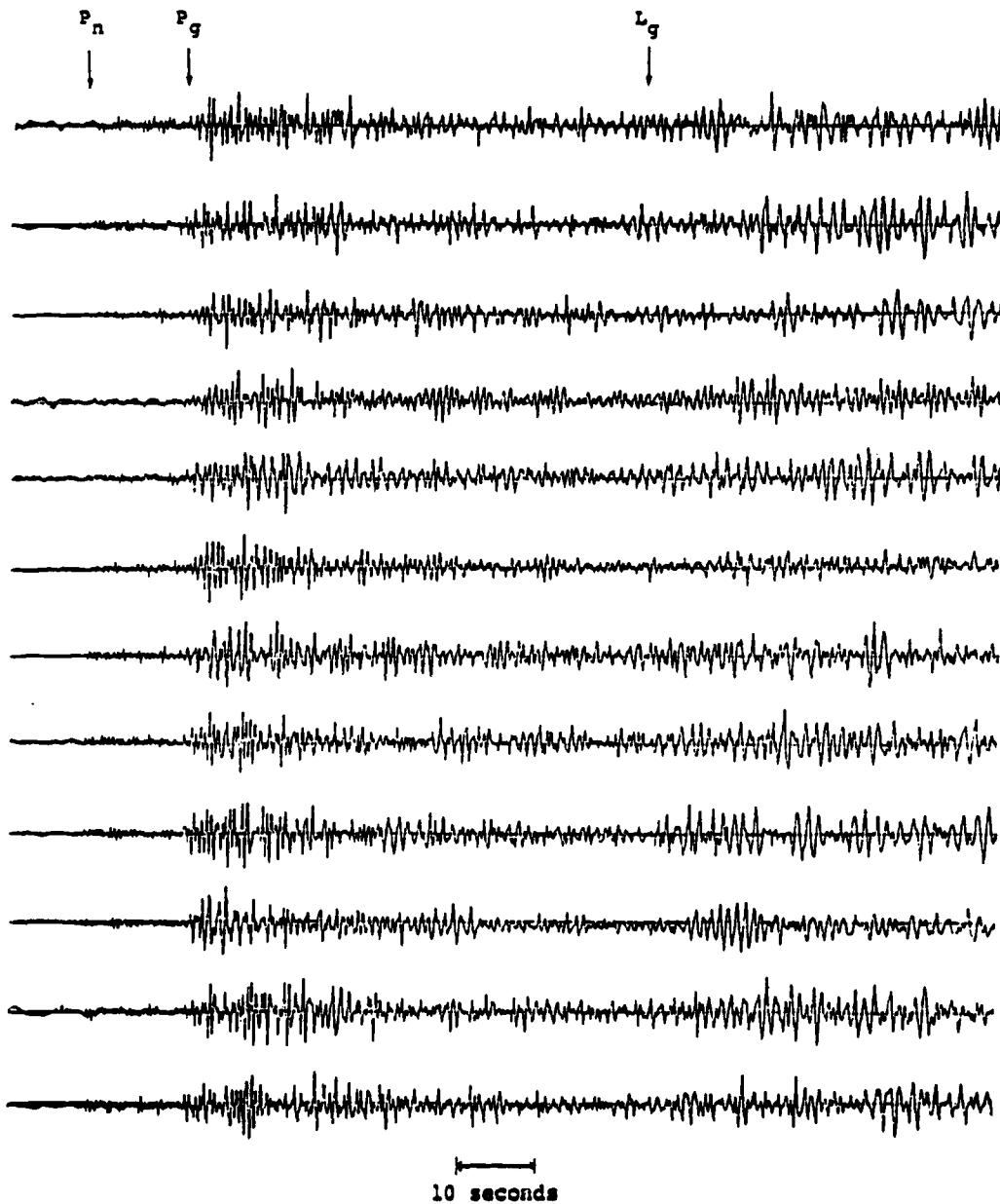


Figure 2. Representative sample ($3.7 \leq m_b \leq 4.3$) of vertical-component, short-period seismograms recorded at station TFO from NTS explosions.

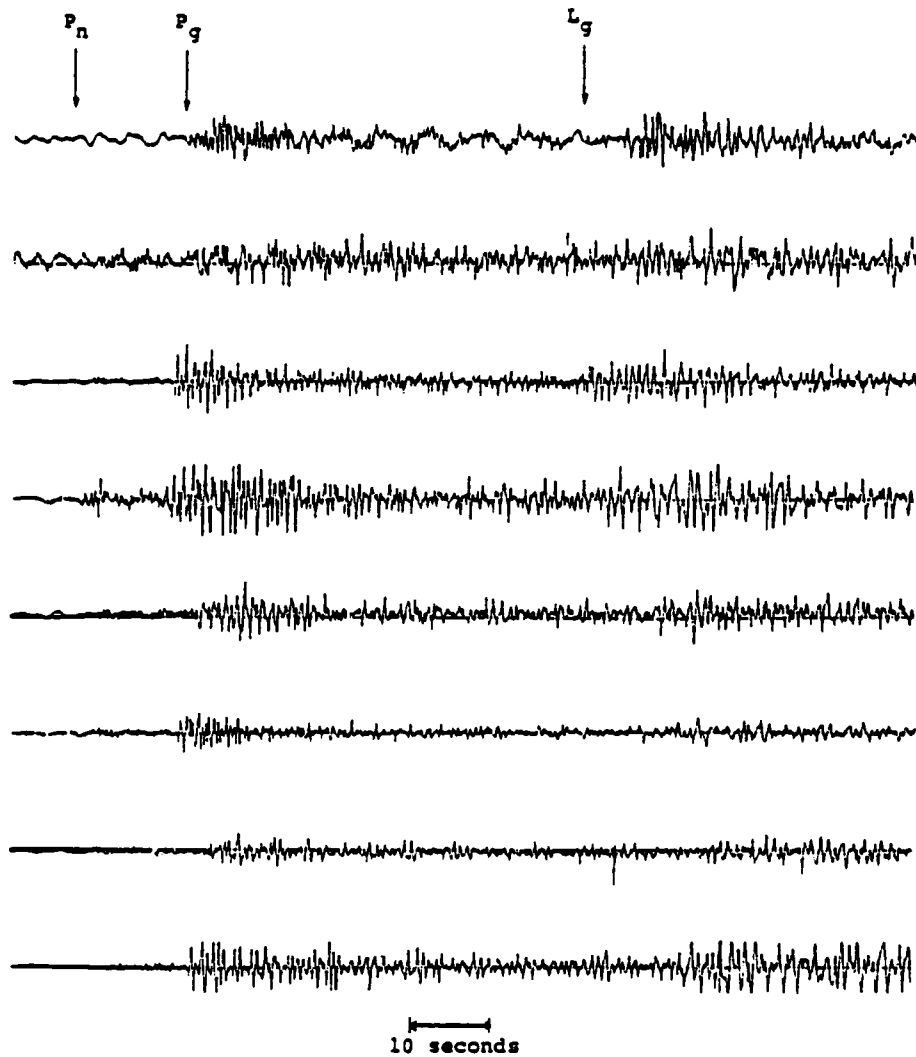


Figure 3. Representative sample ($3.7 \leq m_b \leq 4.3$) of vertical-component, short-period seismograms recorded at station TFO from earthquakes located near NTS.

earthquake signatures are quite similar to those of the explosions shown in Figure 2, although there is an apparent tendency for the earthquake L_g phases to be more distinct. This has been noted before (e.g. Blandford, 1981) and has led to speculation that a simple, time domain L_g/P amplitude ratio might separate the two source types. However, as has been noted previously (Bennett et al., 1981), this proposed discriminant is not reliable when applied to the TFO data. This is illustrated in Figure 4 which shows a plot of maximum P_n amplitude versus maximum L_g amplitude for a large sample of NTS explosions and nearby earthquakes recorded at TFO. It can be seen that the data are intermingled and offer little promise for their use in discrimination. Similar results are found when other P phases are used. This is illustrated in Figure 5 which shows the observed vertical-component, short-period seismograms from an explosion and two nearby earthquakes of about the same magnitude. Clearly, any selected L_g/P amplitude ratio for this explosion will be larger than the corresponding ratios obtained for these earthquakes and, consequently, the proposed discriminant would fail to correctly separate the two source types in this case.

This observed failure of the proposed time domain peak amplitude discriminants prompted a more detailed spectral analysis of the regional phase data in an attempt to determine whether a frequency domain discriminant could be defined which would provide more consistent identification of source type. For this purpose, P_n , P_g and L_g time windows, together with pre-signal noise windows, were identified on each recording and Fourier amplitude spectra were computed for the selected sample of earthquakes and explosions using digitized data sampled at 20 samples/second. The P_n , P_g and L_g time windows were taken to be of length 10, 25.6 and 50 seconds and were associated with onset group velocities of 8.0, 6.0 and 3.6 km/sec respectively. The P_g onset time, which is the least

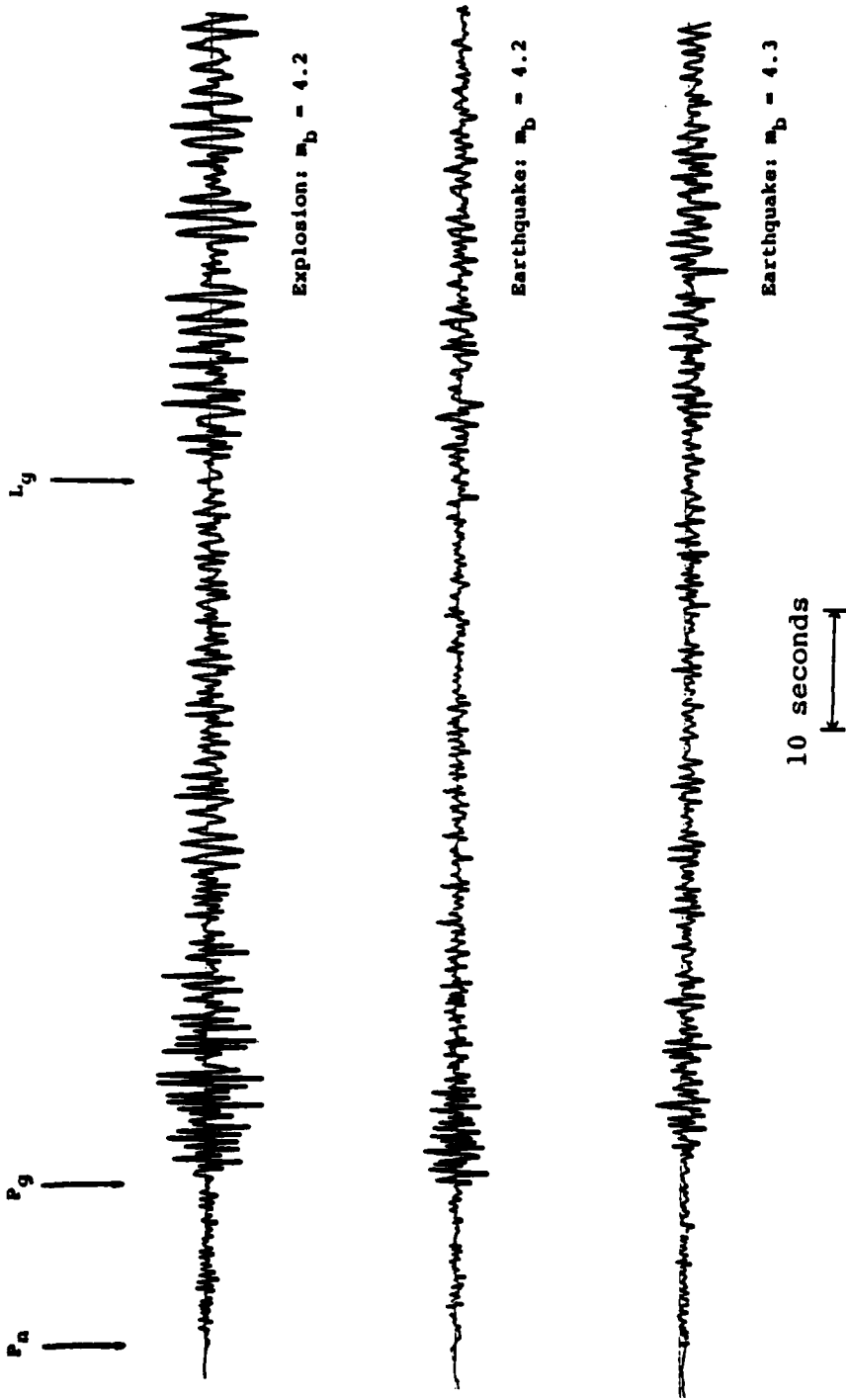


Figure 5. Comparison of vertical-component seismograms recorded at TFO from an explosion and two nearby earthquakes of about the same magnitude.

ambiguous on these records, was visually identified and then the P_n and L_g onset times were determined from the relations:

$$t_{P_g} - t_{P_n} = \frac{\Delta}{6} - \frac{\Delta}{8} - 6$$

$$t_{L_g} - t_{P_g} = \begin{cases} \frac{\Delta}{3.6} - \frac{\Delta}{6} - 5 & \text{(earthquakes)} \\ \frac{\Delta}{3.6} - \frac{\Delta}{6} + 5 & \text{(explosions)} \end{cases}$$

where Δ is the epicentral distance in km and the constants were selected to provide reasonable windows for those events in which the various onset times were easily identifiable. Finally, the noise window was defined to consist of the 6.4 seconds of data immediately prior to the selected P_n window. Note that the $L_g - P_g$ time interval has been taken to be 10 seconds longer for the explosions than for earthquakes at comparable epicentral distances. It seems likely that this observed offset is related to differences in focal depth (cf. Pomeroy, 1980). For purposes of illustration, it might be noted that for explosions at NTS, Δ is essentially constant at an average value of about 530 km and, consequently, $t_{P_g} - t_{P_n} \approx 16$ seconds while $t_{L_g} - t_{P_g} \approx 64$ seconds.

Due to differences in the lengths of the time windows, the spectral sampling for the successive windows (i.e. noise, P_n , P_g , L_g) is twice as dense as for the one immediately preceding. Consequently, the signal spectra have been smoothed to the same effective resolution as the noise spectrum (i.e. about 0.15 Hz) by convolving the raw spectra with a triangular smoothing operator using the algorithm:

$$\tilde{A}_i = \alpha_0 A_i + \sum_{n=1}^{N-1} \alpha_n (A_{i-n} + A_{i+n}) \quad i = N, 2N, 3N, \dots$$

where \tilde{A}_i denotes the smoothed spectral estimates corresponding to the raw spectral values A_i and the α_n are the smoothing coefficients fixed by the requirement that the area under the triangle be equal to unity:

$$\alpha_n = \frac{N-n}{N^2} \quad n=0,1,\dots,N-1$$

with $N = 2,4,8$ for P_n , P_g and L_g respectively. Typical regional phase spectra for an explosion and nearby earthquake of about the same body wave magnitude (as seen through the TFO short-period instrument) are shown in Figure 6 where they can be compared with the background noise spectra measured just prior to the respective P_n arrival times. It can be seen that, for these examples, while the signal-to-noise ratios (S/N) are quite good in the frequency band between about 0.5 and 5.0 Hz, they are not consistently good outside this range. The generality of this observation is illustrated more graphically in Figures 7 and 8 which show the average S/N as a function of frequency (and associated standard errors of estimate in the average, σ) for the P_n , P_g and L_g phases for the earthquake and explosion samples respectively. Again, it can be seen that while the sampling rate provides information on frequency components up to 10 Hz, the S/N ratios are such that usable information is consistently available only in the 0.5 to 5.0 Hz range. Consequently, this frequency band has been adapted for purposes of the present analysis.

In order to gain some insight into possible differences in the spectral composition of regional phases from earthquake and explosion sources, the subset of the sample consisting of the 8 earthquakes and 13 explosions from Tables 1 and 2 with magnitudes in the common range of $3.7 \leq m_b \leq 4.3$ were selected for preliminary analysis. For each phase, all the spectra for a given event type were normalized to the same maximum spectral amplitude level and averaged using only those spectral values

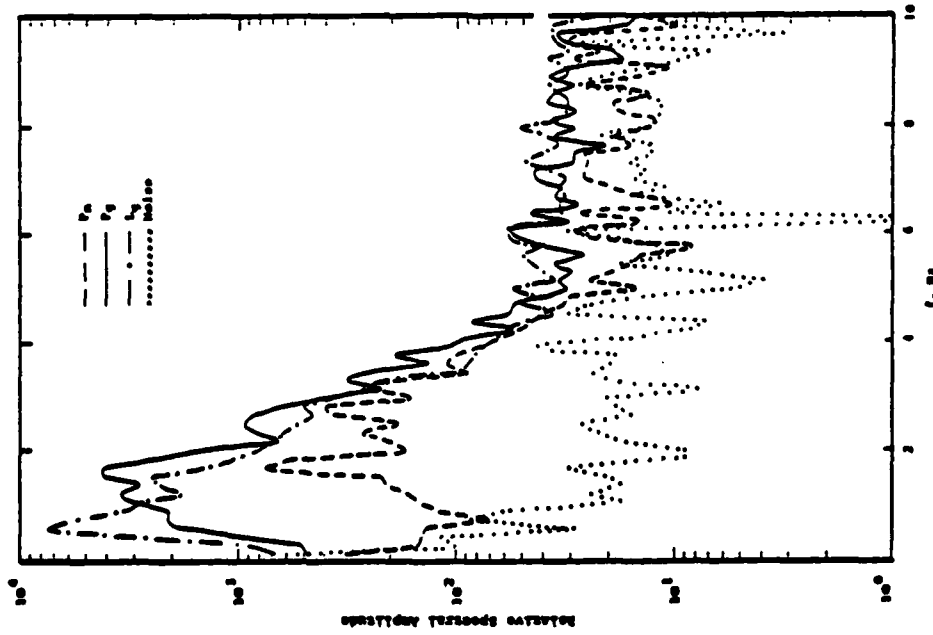
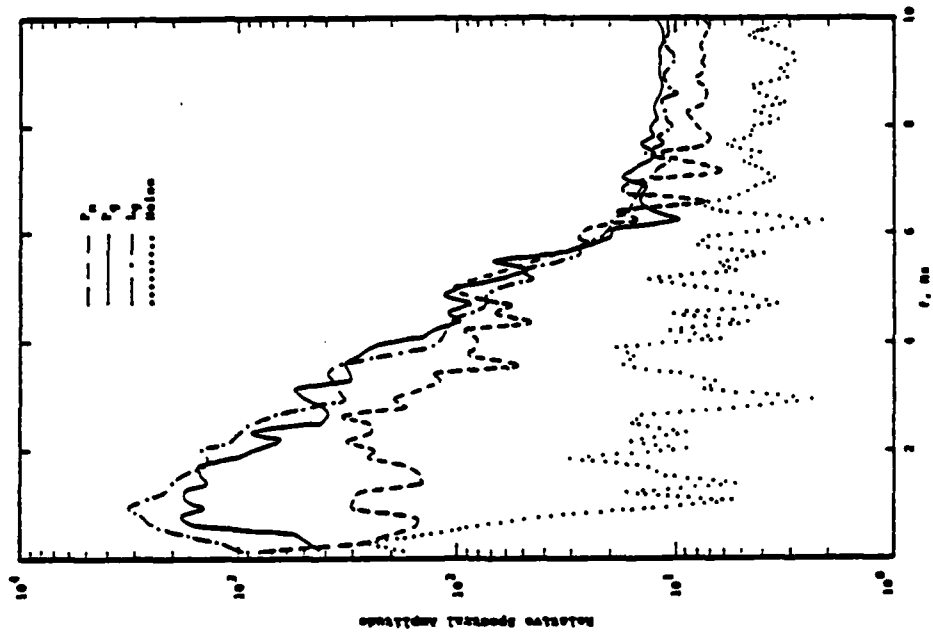


Figure 6. Comparison of regional phase spectra observed at TFO from an explosion (Rivet III, left) and an earthquake (3/23/70, right) of about the same magnitude.

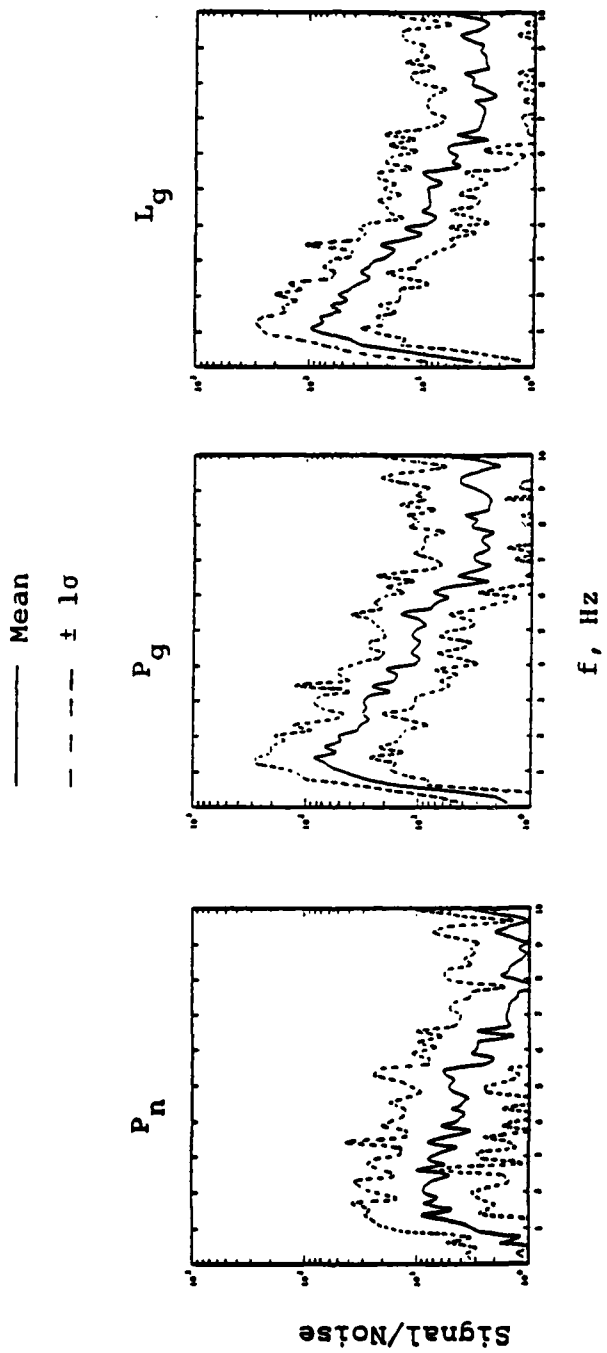


Figure 7. Average S/N as a function of frequency for P_n, P_g and L_g phases recorded at TFO from the selected NTS earthquake sample. Dashed lines denote one standard error of estimate in the mean (σ).

— Mean
 - - - $\pm 1\sigma$

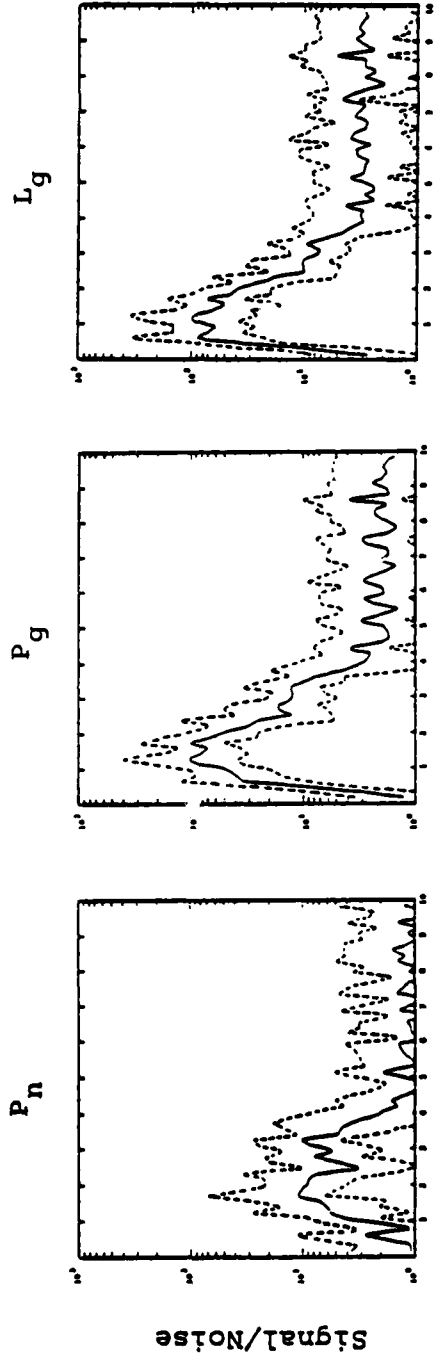


Figure 8. Average S/N as a function of frequency for P_n , P_g and L_g phases recorded at TFO from the selected NTS explosion sample. Dashed lines denote one standard error of estimate in the mean (σ).

for which $S/N > 2$. The results for the P_n phase are shown in Figure 9 where it can be seen that the average spectral shapes associated with the two source types are indistinguishable within the rather large uncertainty in the mean values. The corresponding average P_g spectra are compared in Figure 10 where it can be seen that the mean spectral shape associated with the two source types are quite different, with the average earthquake P_g spectrum being noticeably richer in high frequency content. However, the individual spectra are fairly widely scattered about the average trends, as evidenced by the fact that the standard errors of estimate in the means (σ) overlap over virtually the entire frequency range. Thus, the observed P_g spectral differences do not appear to be consistent enough to completely separate the two populations. It might be noted that the differences in P_g spectra shown in Figure 10 appear to be in conflict with the findings of Bakun and Johnson (1970) who concluded that NTS explosion P_g spectra are relatively richer in the frequency band 1.35 to 2.0 Hz than corresponding earthquake P_g spectra. However, as Peppin (1976) has noted, their conclusion was based on data observed from earthquakes which are generally located at substantial distances away from NTS. In fact, Peppin (1976) claims that when data from more proximate earthquakes are examined, there is not much difference in this frequency band, consistent with the results shown in Figure 10.

The average earthquake and explosion L_g spectra are compared in Figure 11 where it can be seen that they show differences very similar to those noted for P_g , indicating that the average earthquake L_g phase is richer in high frequency content than the corresponding average explosion L_g phase having the same maximum spectral amplitude level. Moreover, unlike the P_g spectra, the variability of the earthquake and explosion L_g spectra about their respective means is quite small and, in fact, the differences in average spectral content are seen to

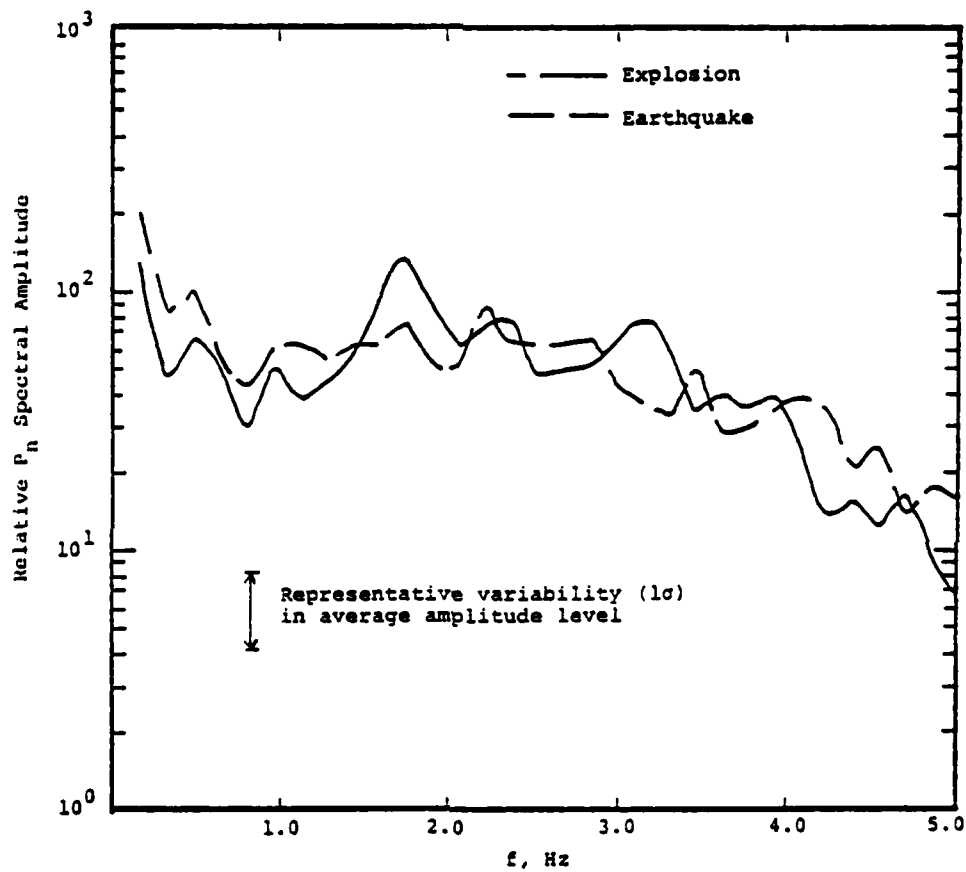


Figure 9. Comparison of average earthquake and explosion P_n spectra ($3.7 \leq m_b \leq 4.3$) derived from NTS events recorded at TFO.

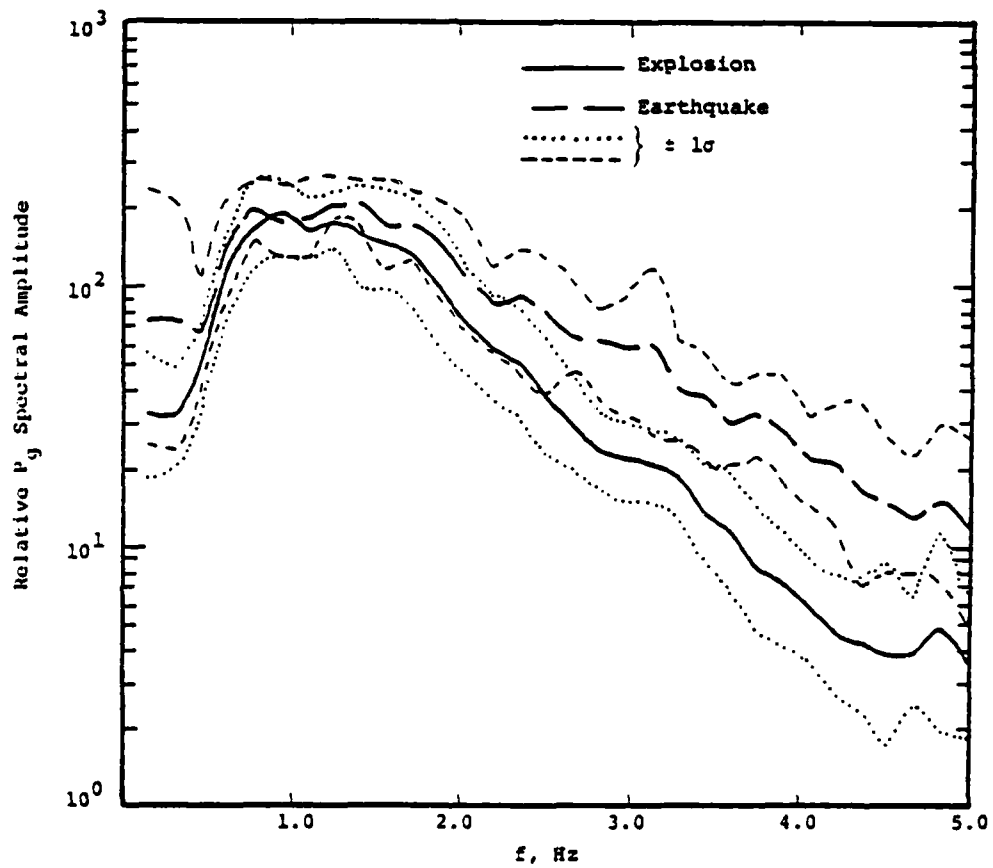


Figure 10. Comparison of average earthquake and explosion P_g spectra ($3.7 \leq m_b \leq 4.3$) derived from NTS events recorded at TFO.

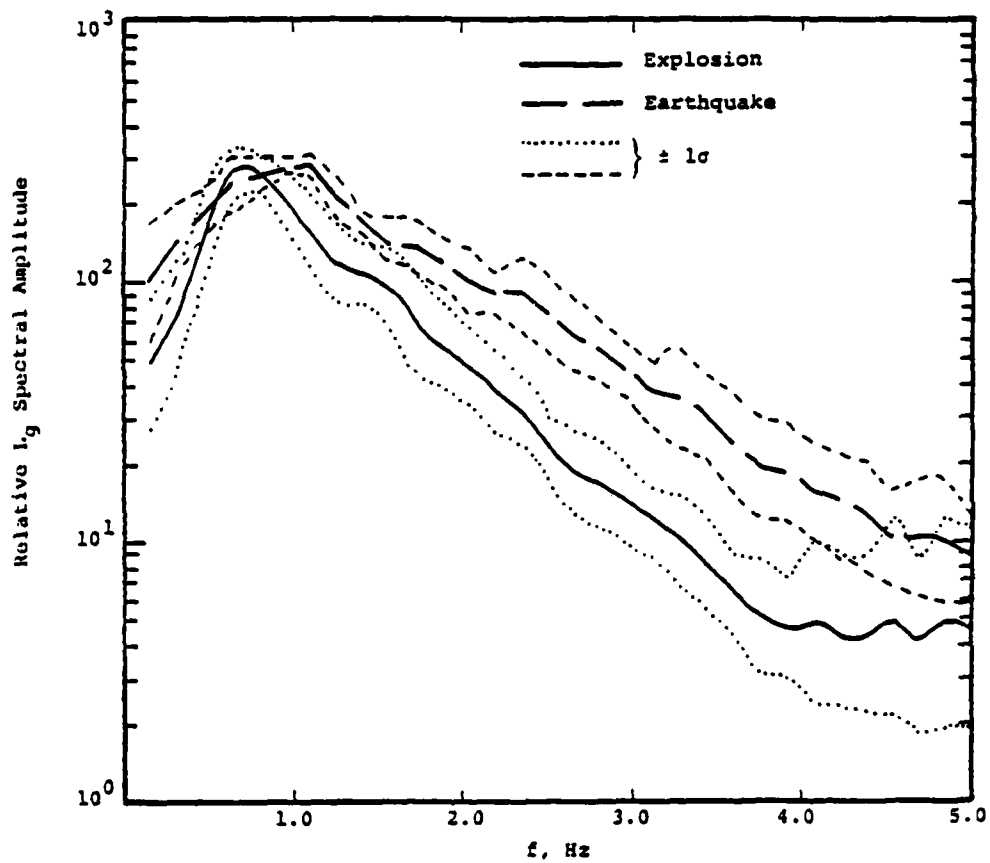


Figure 11. Comparison of average earthquake and explosion L_g spectra ($3.7 \leq m_b \leq 4.3$) derived from NTS events recorded at TFO.

be statistically significant over the frequency range from about 2.0 to 4.0 Hz. On the basis of these observations, a tentative L_g spectral discriminant has been defined as the ratio of the average spectral amplitude level in the 0.5 to 1.0 Hz passband to the average spectral amplitude level in the 2.0 to 4.0 Hz passband, again, the averages being computed only over those spectral values for which $S/N > 2$. The value of this ratio for the 13 explosions and 8 earthquakes in the common magnitude range of $3.7 \leq m_b \leq 4.3$ are compared in Figure 12 where it can be seen that good separation of the two populations has been obtained. Since there is no obvious indication of magnitude dependence in Figure 12, the same L_g spectral ratios have been computed for the entire set of earthquakes and explosions in Tables 1 and 2 and are plotted as a function of magnitude ($3.3 \leq m_b \leq 4.8$) in Figure 13. It can be concluded from this figure that the proposed L_g spectral discriminant is quite promising, showing an average separation of the two populations of more than a factor of 3. The only clearly anomalous point is the value for the Massachusetts Mountain earthquake (8/5/71) at $m_b = 4.3$ which plots up within the lower bound on the explosion population in Figure 13. A re-examination of the data from this event indicates that the L_g signal is in fact moderately clipped. Although to a first degree of approximation clipping would be expected to decrease rather than increase the value of the spectral ratio shown here, the fact that it occurred indicates that the data are uncertain to some extent. Possible evidence of this will be provided in the following discussion in which Massachusetts Mountain earthquake data recorded at a different near-regional station will be shown to be quite consistent with the average L_g spectral discriminant separation shown in Figure 13.

Given the initial success with the vertical component data described above, a similar analysis of the horizontal component data measured from events in the common magnitude

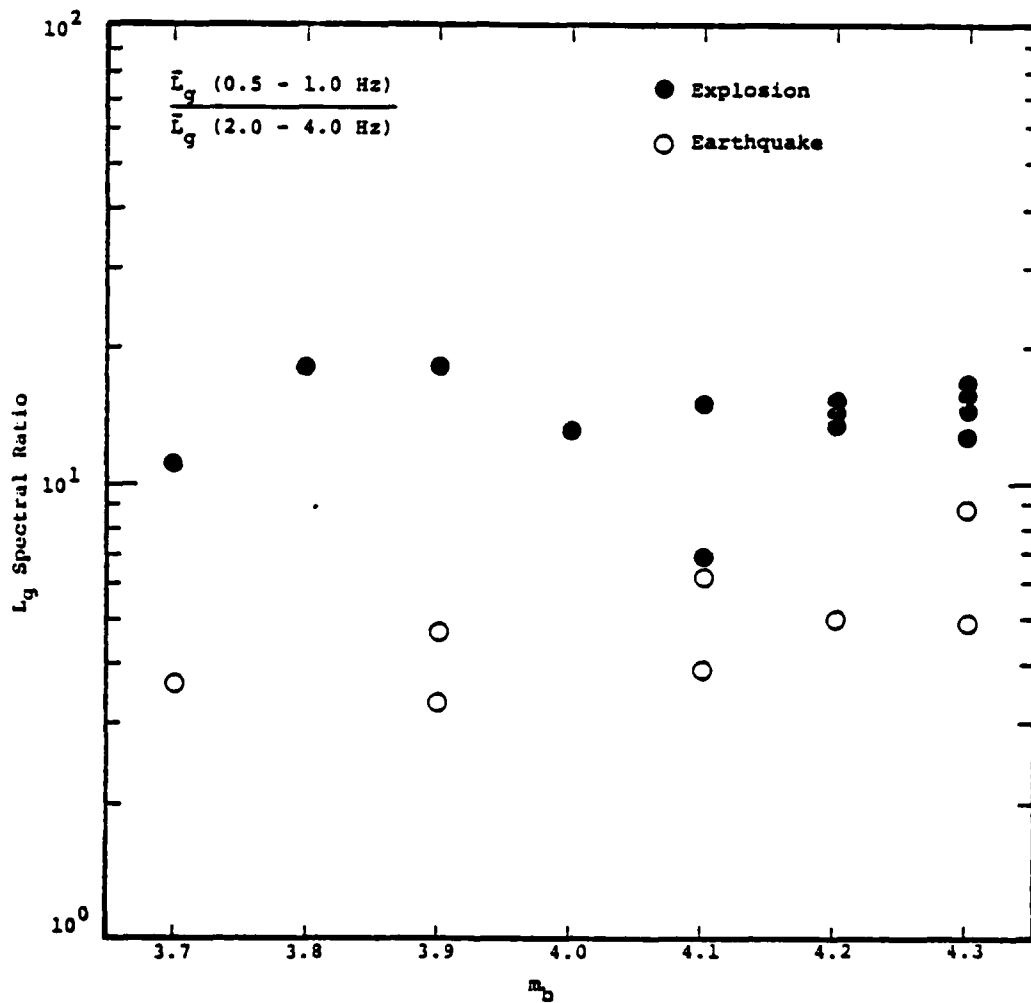


Figure 12. Comparison of vertical-component L_g spectral ratio discriminant (ratio of average amplitude levels in 0.5 to 1.0 Hz and 2.0 to 4.0 Hz passbands) for NTS explosions and earthquakes ($3.7 \leq m_b \leq 4.3$).

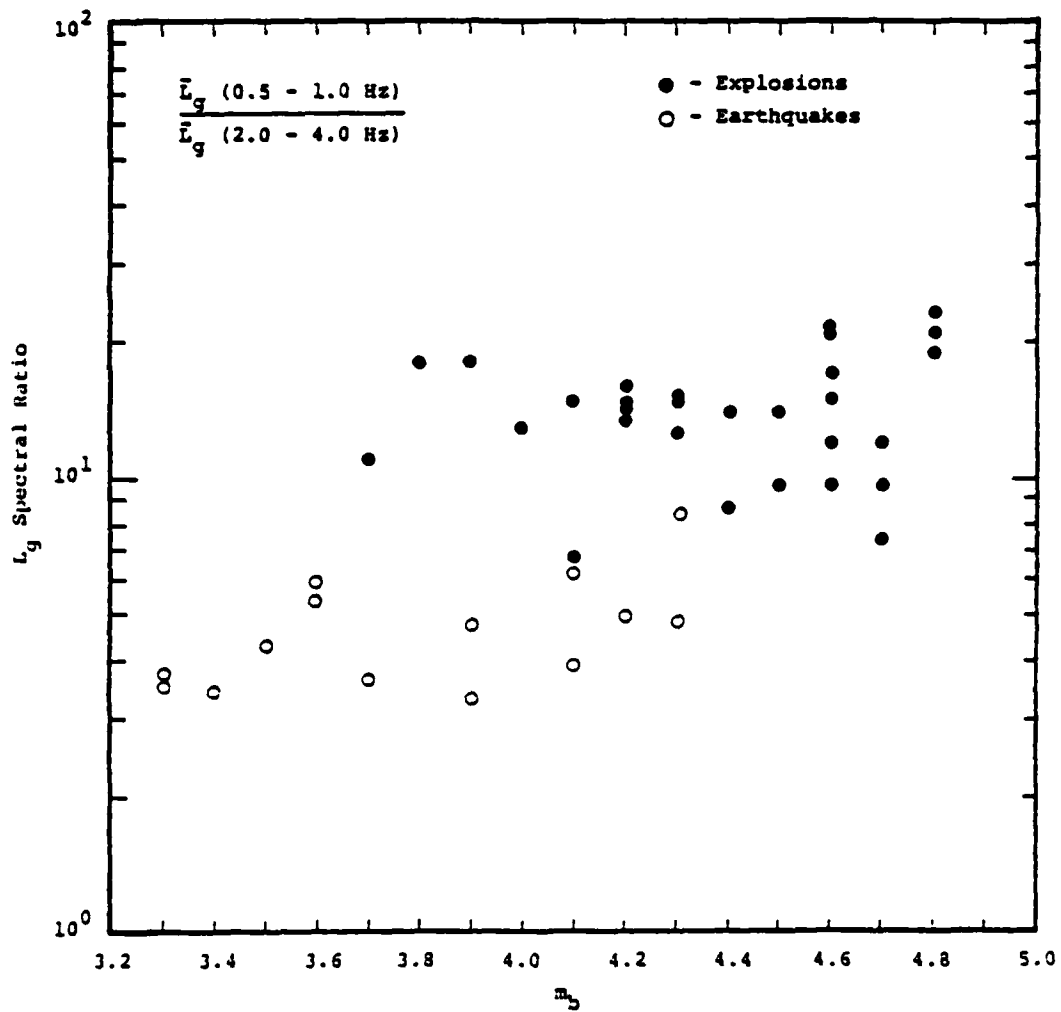


Figure 13. Comparison of vertical-component L_g spectral ratio discriminant (ratio of average amplitude levels in 0.5 to 1.0 Hz and 2.0 to 4.0 Hz pass-bands) for NTS explosions and earthquakes ($3.3 \leq m_b \leq 4.8$).

range of $3.7 \leq m_b \leq 4.3$ has been performed. The available sample is somewhat smaller in this case (5 earthquakes, 13 explosions) than in the case of the vertical component data, due to the fact that horizontal component recording at TFO was discontinued during the time interval from which the sample was collected. The horizontal component data were originally recorded on instruments oriented north/south and east/west and consequently a rotation of axes was performed using the digital data to obtain horizontal motions oriented radial (R) and transverse (T) with respect to the approach azimuth at TFO from events near NTS. Spectra for the P_n , P_g , L_g and noise windows were then computed using the same procedures employed with the vertical component data and the spectra from the two source types were normalized and averaged as described above. It was found that the relative spectral shapes on the horizontal components are essentially identical to those inferred from the vertical component recordings. This is illustrated in Figure 14 which shows a comparison of the average earthquake and explosion L_g spectral shapes deduced from the three orthogonal components of motion. It can be seen that the average horizontal component spectra are remarkably consistent with the average vertical component spectra, again indicating that the earthquake L_g phase is richer in high frequency content than the corresponding explosion L_g phase. The L_g spectral ratio discriminant described above in conjunction with the analysis of the vertical component data has also been applied to these horizontal component data and the results are shown in Figure 15 where they are compared with the subset of the vertical component results consisting of those events recorded on all three components of motion. It can be seen that, at least for this limited sample, the proposed L_g spectral discriminant appears to work as well for the horizontal component data as it does for the vertical component data.

Thus, there is strong evidence based on a well-controlled data set, that NTS explosions and nearby earthquakes in the

— Explosion
- - - Earthquake

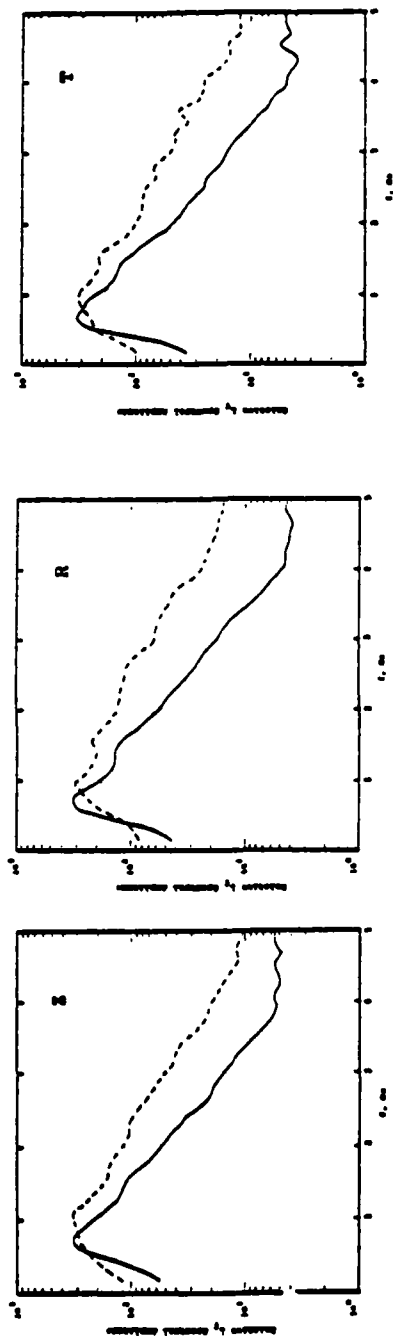


Figure 14. Comparison of vertical (Z), radial (R) and tangential (T) component average earthquake and explosion Lg spectra derived from NTS events recorded at TFO.

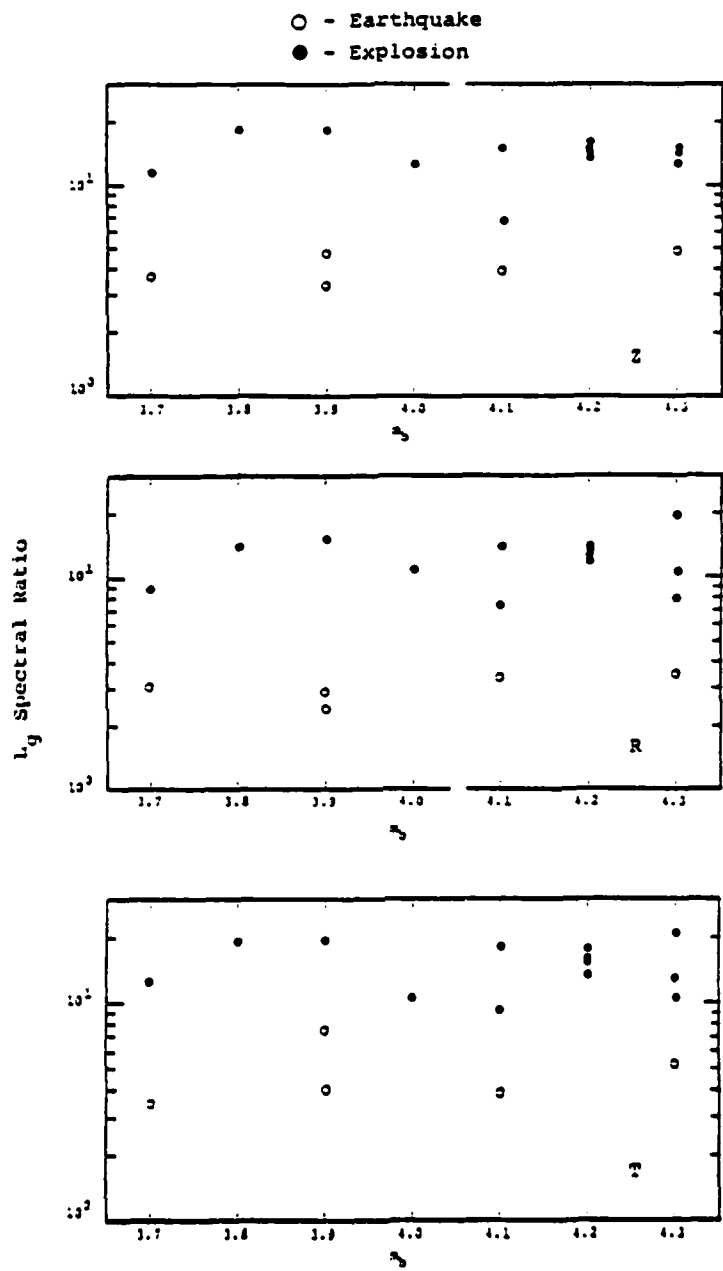


Figure 15. Comparison of vertical (Z), radial (R) and tangential (T) component L_g spectral ratio discriminant for NTS explosions and earthquakes.

magnitude range $3.3 \leq m_b \leq 4.8$ can be identified on the basis of an L_g spectral discriminant which is based on the fact that typical earthquake L_g spectra are richer in high frequency (2.0 - 4.0 Hz) spectral content than typical explosion L_g spectra having the same low frequency (0.5 - 1.0 Hz) spectral amplitude level. This has been noted before (Murphy, 1975), in conjunction with an analysis of a small sample of near-regional, broadband seismic data recorded in the vicinity of NTS. For example, Figure 16 compares broadband and bandpass filtered time histories computed from data recorded at Tonopah, Nevada ($\Delta \approx 170$ km) from the Massachusetts Mountain earthquake (E075, 8/5/71) and a nearby NTS explosion (denoted #235) of the same magnitude (Murphy, 1975). Note that, although the spectral amplitude level in a narrow band around a center frequency of 6.6 Hz for the earthquake and explosion is comparable for the initial P waves, the spectral amplitude level for the phases following S_n is significantly greater for the earthquake than for the explosion, in agreement with the average TFO results shown above. It is significant that the earthquake recording shown in this figure is from the same event (8/5/71) which failed to discriminate at TFO (cf. Figure 13). This provides additional evidence which suggests that the TFO anomaly may be related to data recording problems (i.e. clipping on this event) as opposed to the event itself being anomalous.

Additional evidence concerning the proposed discriminant is provided by the recent study of Gupta and Blandford (1981) who noted comparable diagnostic differences in the spectral composition of the L_g phases recorded from the Eastern U.S. Salmon explosion and the nearby Alabama earthquake of 2/8/64. This suggests that the observed L_g spectral differences are not due to any peculiarities of the NTS to TFO propagation path or to unusual source characteristics of Yucca Flat explosions in alluvium and tuff. That is, there

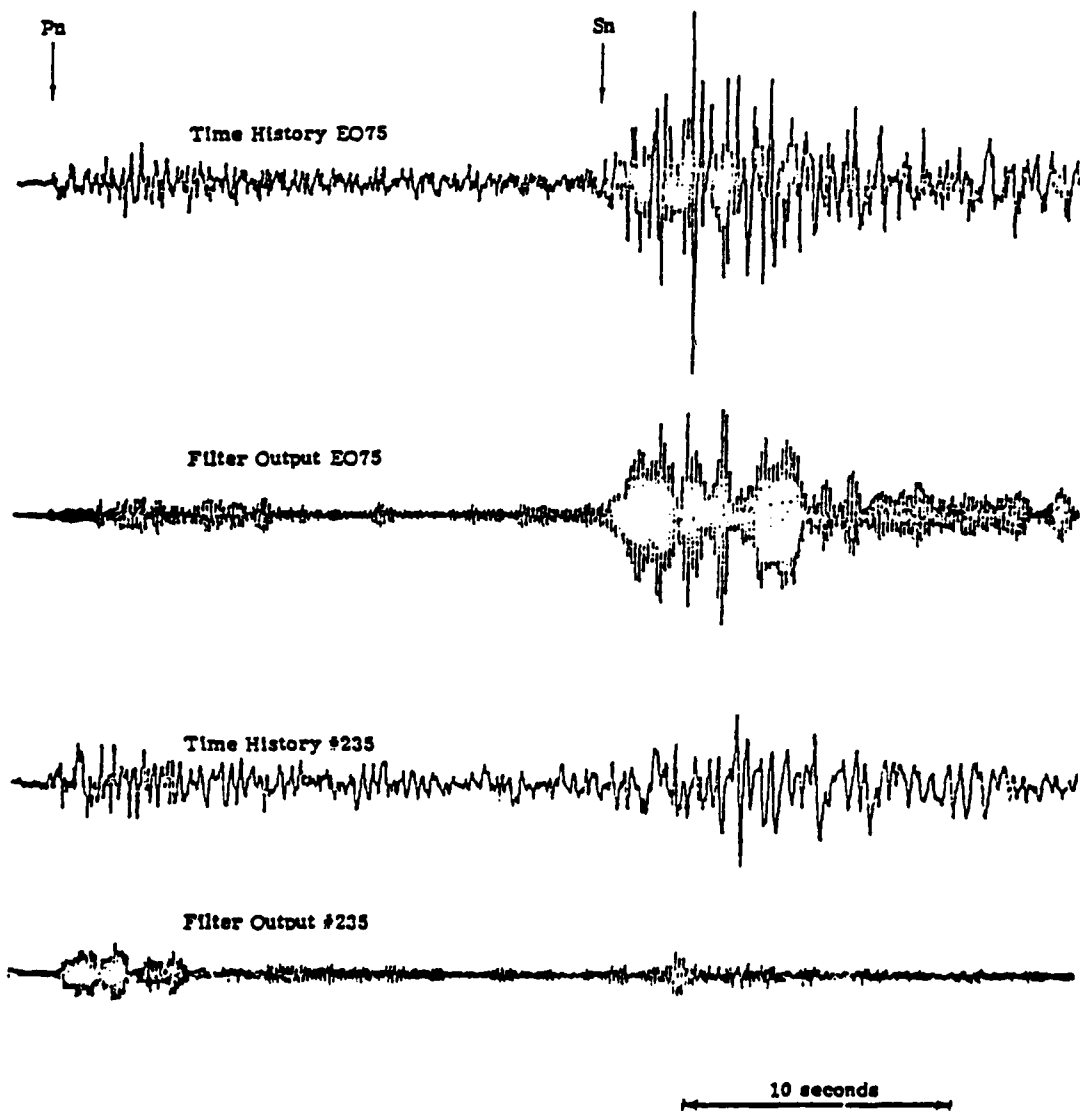


Figure 16. Comparison of broadband and bandpass filtered ($f_c \approx 6.6$ Hz) time histories computed from data recorded at Tonopah, Nevada ($\Delta \approx 170$ km) from the Massachusetts Mountain earthquake (EO75, 8/5/71) and a nearby NTS explosion (#235) of the same magnitude (Murphy, 1975).

is evidence that the L_g spectral differences persist for explosions in hardrock source environments (i.e. salt) over Eastern U.S. propagation paths typical of the areas of interest in seismic monitoring.

A preliminary attempt has been made to derive a quantitative understanding of this difference in L_g spectral composition between the two source types using the theoretical L_g synthesis model described by Bache et al. (1981). The starting point for these investigations has been the observation that, while the spectra of the P_g phases measured from the two source types show differences similar to those associated with L_g , the corresponding P_n spectra do not (cf. Figures 9-11). This suggests that the observed differences in L_g spectral composition may be related to characteristic differences in the focal depths and/or focal mechanisms of the two source types. Consequently, the initial investigations have focused on analyses of the effects of these two variables. The crustal model used in these simulations is summarized in Table 3. This model is a modified version of the average Basin and Range structure proposed by Priestly and Brune (1978), with low-velocity surficial layers added to represent the Yucca Flat explosion source environment. Synthetic L_g spectra have been computed by superposing the first 35 Rayleigh modes for this structural model, assuming a series of different earthquake and explosion sources. Both the explosions and earthquakes have been modeled as point sources (center of compression and double couple respectively) with step function time dependence; and, consequently, possible differences in source time functions or source-finiteness effects are not considered. For purposes of comparison with the observations, it has been assumed that the observation point is at a range of 500 km (i.e. the average range from TFO to NTS) and that the L_g data have been measured with a standard LRSM short-period seismometer.

Figure 17 shows a comparison of the vertical-component

TABLE 3
 BASIN AND RANGE STRUCTURAL MODEL

<u>Layer</u>	<u>Thickness, km</u>	<u>α km/sec</u>	<u>β km/sec</u>	<u>ρ gm/cm³</u>	<u>Q</u>
1	0.35	2.03	1.03	1.70	20
2	0.11	2.40	1.45	1.90	20
3	0.23	4.40	2.75	2.20	100
4	1.81	5.00	3.10	2.40	400
5	22.5	6.10	3.57	2.80	800
6	10.0	6.60	3.85	2.84	1000
7	∞	7.80	4.50	3.30	1600

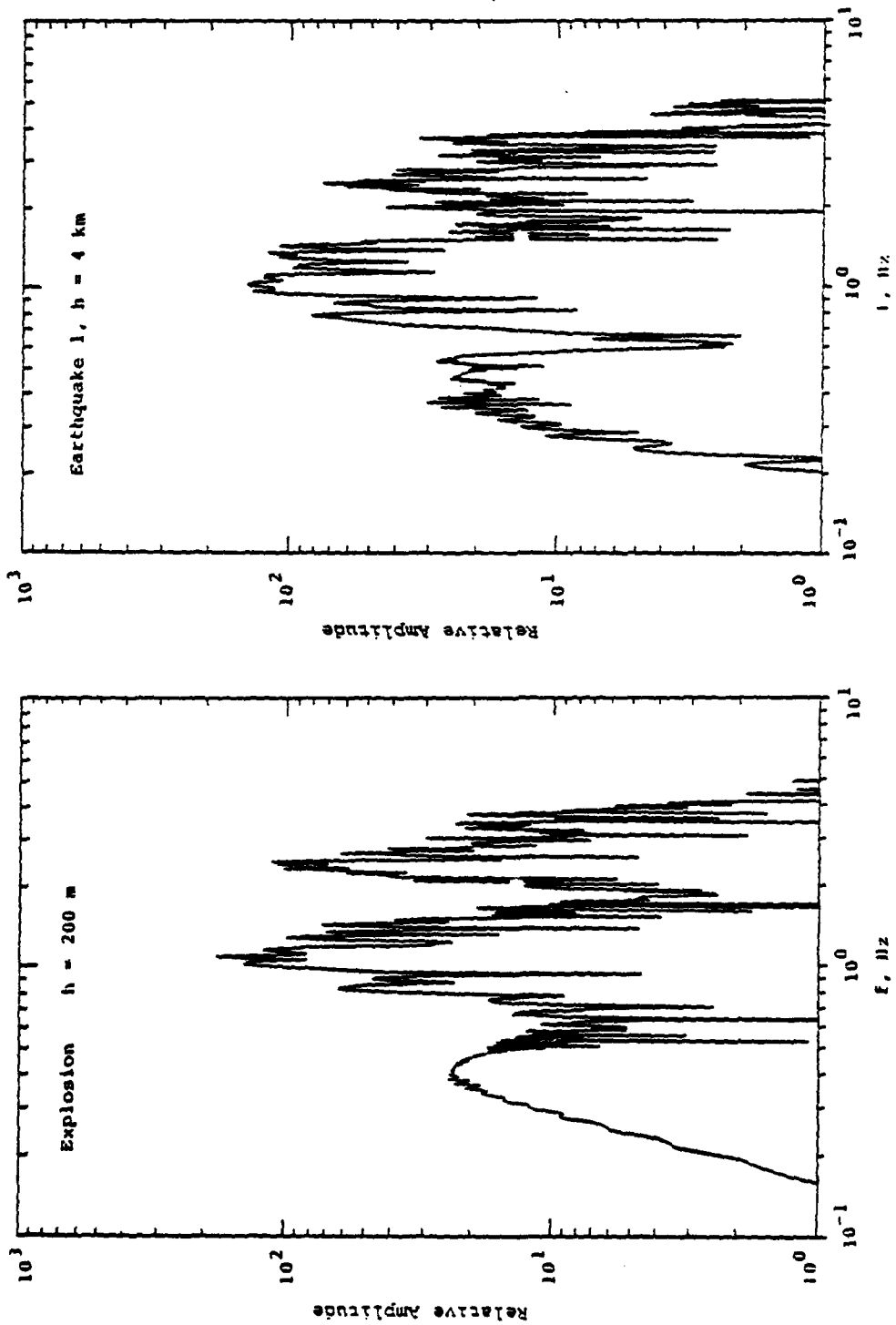


Figure 17. Comparison of theoretical Lg spectra from a shallow explosion (left) and an earthquake (right) with a focal depth of 4 km.

L_g spectrum predicted for an explosion at a depth of 200 m in tuff with that predicted for a strike-slip earthquake on a vertical fault plane at a depth of 4 km in the underlying basement. For the earthquake, it has been assumed that the observation point is located at an azimuth of 22.5° from the strike direction. The first thing that can be noted from this figure is that the overall shapes of the synthetic L_g spectra do not agree very well with the observed spectra shown in Figure 11. In particular, the synthetic spectra show a strong peak in the 2-3 Hz band which is noticeably missing from the observations. This suggests that the adopted crustal model, which corresponds to an average Basin and Range structure, is probably not very representative of the propagation path between NTS and TFO. However, Bache et al. (1981) have shown that the effects of focal depth and focal mechanism on L_g are not strongly dependent on the particular structural model employed and, consequently, any characteristic differences due to these source factors should show up in a comparison of the two spectra, even if the individual spectral shapes are not representative of the observed data. However, it can be seen from Figure 17 that the explosion and earthquake spectral shapes are quite consistent in this case, showing no evidence of the pronounced difference in high frequency spectral content noted in the analysis of the observed TFO data. Figure 18 shows a comparison of the earthquake L_g spectrum from Figure 17 with the spectra predicted for the same source mechanism at focal depths of 7 and 10 km. It can be seen that there is no indication that changes in focal depth over the depth range thought to be representative of the TFO earthquake data sample have a pronounced effect on the L_g spectral composition. Figure 19 shows a comparison of the earthquake L_g spectrum from Figure 17 with that predicted for an event with the same depth, but somewhat different focal mechanism (i.e. slip at an angle of 20° from the horizontal on a plane dipping

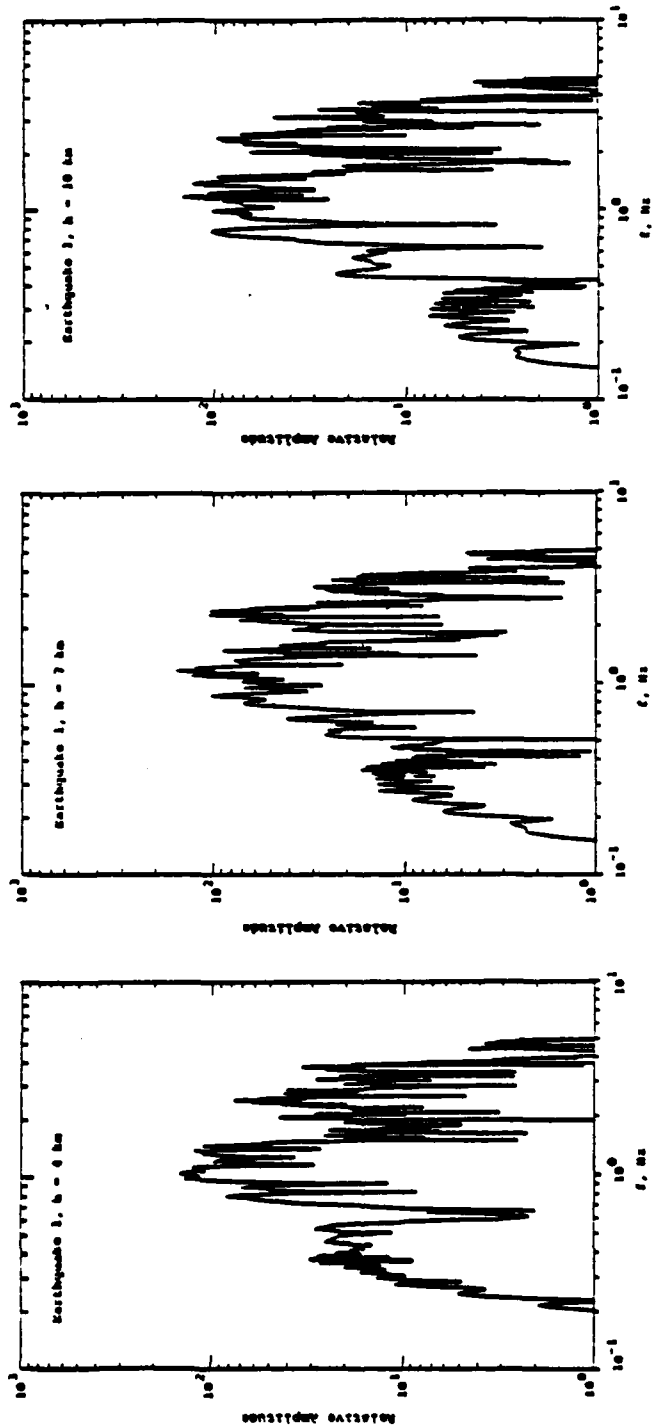


Figure 18. Comparison of theoretical Lg spectra computed for the same earthquake at focal depths of 4, 7 and 10 km.

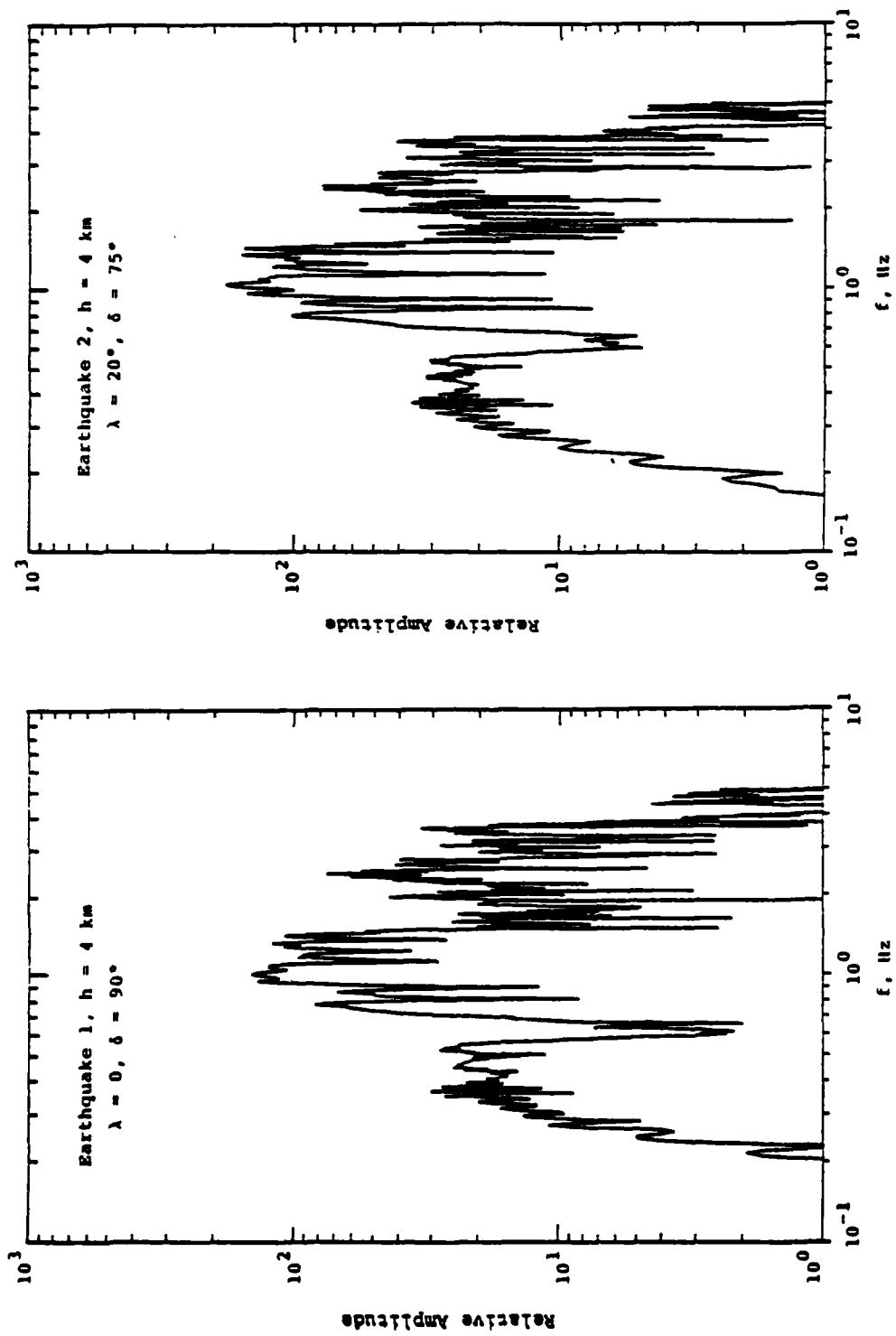


Figure 19. Comparison of theoretical L_q spectra computed for two earthquakes with the same focal depth (4 km) but different focal mechanisms.

75°). Again, the two spectra are essentially identical, indicating that the L_g spectral shape is relatively insensitive to minor perturbations about the inferred dominant focal mechanism for the area (i.e. strike-slip motion on steeply dipping faults).

Thus, these preliminary attempts to synthetically reproduce the observed dependence of L_g spectral shape on source type using the theoretical L_g model proposed by Bache et al. (1981) have been unsuccessful. However, additional modeling will be required before definitive conclusions can be reached. The most obvious modification to the simulations presented above would be to use an alternate crustal model more appropriate to the average propagation path from NTS to TFO in an attempt to obtain synthetic L_g spectral shapes which agree better with the observed data. A more subtle problem concerns the use of extremely low Q values (i.e. 20) to model inelastic effects in the near-surface layers of the structural model given in Table 3. The choice of these low Q values is dictated primarily by the need to suppress the fundamental Rayleigh mode contribution to the motion which tends to dominate the synthetic time histories, but is conspicuously missing from the observed data. However, the actual physical mechanism by which this fundamental mode energy is dispersed is probably more closely related to scattering and mode conversion at near-surface, lateral heterogeneities than to inelastic attenuation, and the manner in which this is modeled may have a significant influence on the shape of the synthetic spectra. Thus, more sophisticated theoretical models may be required to adequately model the observed L_g data from shallow sources.

III. TIME-DOMAIN MEASUREMENTS OF LONG-PERIOD PHASES AT REGIONAL DISTANCES

Historically, most attempts to discriminate earthquakes and explosions have focused on simple time-domain measurements. One of the most potent discriminants of this type has proven to be M_s versus m_b which exploits differences in the long-period and short-period seismic wave motion produced by the different kinds of events. In principle, seismic waves from earthquakes, because of the distributed nature of their source and the rupture process involved in their generation, are expected to produce a relatively high proportion of long-period energy compared to explosions with equivalent short-period energy. Thus, taking m_b and M_s as measures of the short-period energy and long-period energy respectively, earthquakes would be expected to produce larger M_s values than explosions with the same m_b . The rationale we've just presented is somewhat simplified. As magnitude decreases the physical extent of the earthquake source decreases. Furthermore, current understanding of the physics of the earthquake rupture process does not preclude the possibility of rapid, short-term movements which could make the earthquake source term appear explosion-like. As a result, there has been a long-standing question about whether the M_s/m_b discriminant, which has generally proven to be quite reliable at large magnitude, can be extended to low magnitude levels.

This question has been addressed in previous studies by Peppin and McEvelly (1974) and by Lambert and Alexander (1971). Because of the restricted range at which useful signals can be measured for the small natural earthquakes occurring near the Nevada Test Site (NTS), Peppin and McEvelly relied on near regional recordings from broadband instruments at four stations operated by Lawrence Livermore Laboratory at Mina, Nevada ($\Delta \approx 230$ km), Kanab, Utah ($\Delta \approx 430$ km), Landers,

California ($\Delta \approx 440$ km) and Elko, Nevada ($\Delta \approx 500$ km). In addition to explosions and naturally occurring earthquakes, their data set included cavity collapses and explosion after-events which adds some complication to interpretation of the results. They passed the broadband data through high- and low-frequency filters to extract the P_n and long-period Rayleigh wave signals respectively. The dominant periods of the resulting signals were found to be 0.25 and 0.5 sec. for P_n and near 12 sec. for the long-period Rayleigh waves. A comparison of their relative amplitude measurements at two of the stations is shown in Figure 20. Peppin and McEvilly noted that on these plots the explosion afterevents tended to group with the earthquakes. Their principal conclusion was that the separation between explosions and other events in the P_n versus long-period Rayleigh wave amplitude display prevails to magnitudes at least as low as 3 (m_b). The chief criticism of this observation would appear to be the limited magnitude overlap between the earthquake and explosion samples and the small number of tectonic earthquakes (3 each at Mina and Kanab). In fact, if the nontectonic events are eliminated, the results at all stations except Mina suggest a tendency for the earthquake and explosion data sets to converge at lower magnitudes.

Lambert and Alexander (1971) arrived at conclusions similar to those of Peppin and McEvilly using measurements from LRSM and VELA observatory stations for NTS explosions and earthquakes primarily from the Nevada-Utah region but also including events in New Mexico, Colorado, Wyoming, Idaho, Missouri and Alaska. Their principal conclusion was that the surface wave magnitudes from NTS explosions are on the average about 0.62 to 0.65 units smaller than for earthquakes with comparable m_b 's. They suggest that these differences prevail to magnitudes below 3 (m_b). However, it should be noted that their conclusions are pessimistic about the applicability of the discriminant using single-station measurements because of

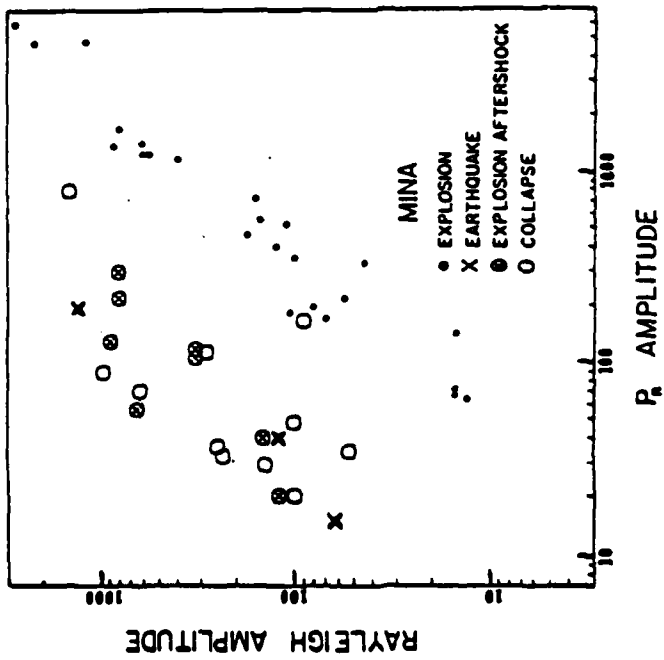
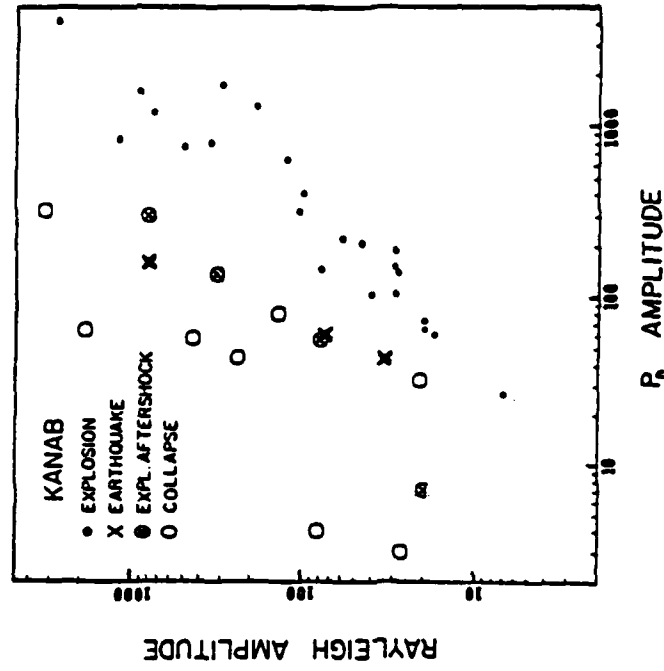


Figure 20. Long-period Rayleigh wave amplitude versus short-period P_n amplitude for an NTS explosion and earthquake sample recorded at MINA and KANAB (after Peppin and McEvilly, 1974).

observed overlap and scatter. The chief limitations in the Lambert and Alexander study would appear to be their use of earthquake sources in some cases quite far removed from NTS and the resultant introduction of uncertain transmission path perturbations. Further, the failure of the discriminant which they noted for single-station measurements is potentially quite important for identification of low-level events which quite possibly will be detected by only one or two stations.

Considering the promise of some of these previous studies and the availability of the Tonto Forest Observatory (TFO) data, we decided to test the reliability of proposed discrimination using amplitude measurements of short- and long-period phases observed at regional distances. The earthquake set, as has been described in the preceding chapter, is well constrained and includes only events located within about 1° of NTS (cf. Figure 1). Because of differences in the dynamic range between the magnetic tape recording system described in Section II and the film records used in the time-domain measurements to be described in this chapter, and between the short- and long-period recording systems, some differences exist between the two data bases. The earthquakes and explosions for which long-period time-domain measurements were made are shown in Tables 4 and 5 respectively. Event times, locations and magnitudes are from the NEIS listings; additional explosion information is from the Springer and Kinnaman reports (1971, 1975). The earthquakes range in body-wave magnitude from somewhere below 3.3 to 4.7 and the explosions from 3.5 to 6.0. The resulting sample overlaps in the magnitude range from 3.5 to 4.7 (m_p) which includes 13 earthquakes and 11 explosions.

The first item of interest was to see if the relatively low magnitude events produced useful long-period signals at TFO. Figure 21 shows examples of the recorded long-period Rayleigh waves. The records are for the vertical components.

TABLE 4
EXPLOSION SAMPLE

<u>Name</u>	<u>Date</u>	<u>Origin Time (UT)</u>	<u>m_b</u>	<u>Yield,**kt</u>	<u>Source Medium</u>
Manzanas	05/21/70	14:00:00.04	3.5	L	Tuff
Effendi	04/27/67	14:45:00.00	3.8	L	Alluvium
Fawn	04/07/67	15:00:00.04	3.9	L	Alluvium
Cyclamen	05/05/66	14:00:00.04	4.2	13	Alluvium
Rivet III	03/02/67	15:00:00.00	4.2	L	Alluvium
Pedernal	09/29/71	14:00:00.04	4.4	L	Tuff
Minute Steak	09/12/69	18:02:20.42	4.5	L	Alluvium
Diana Mist	02/11/70	19:15:00.04	4.6	L	Tuff (Rainier Mesa)
Snubber	04/21/70	14:30:00.04	4.6	L	Tuff
Ildrim	07/16/69	13:02:30.04	4.7	L-I	Tuff
Labis	02/05/70	15:00:00.04	4.7	L-I	Tuff
Lovage	12/17/69	15:15:00.04	4.8	L	Alluvium
Can	04/21/70	15:00:00.04	4.8	L-I	Tuff
Coffer	03/21/69	14:30:00.00	4.9	<100	Alluvium
Pod	10/29/69	20:00:00.04	5.0	L-I	Tuff
Hudson Moon	05/26/70	14:16:00.17	5.0	L	Tuff (Rainier Mesa)
Bourbon	01/20/67	17:40:04.41	5.2	L-I	Limestone
Wineskin	01/15/69	19:30:00.04	5.3	L-I	Tuff (Rainier Mesa)
Nash	01/19/67	16:45:00.14	5.4	L-I	Dolomite
Scotch	05/23/67	14:00:00.04	5.4	150	Tuff (Pahute Mesa)
Pile Driver	06/02/66	15:30:00.09	5.5	~56	Granite (Climax Stock)
Hutch	07/16/69	14:55:00.04	5.6	L-I	Alluvium
Flask	05/26/70	15:00:00.05	5.6	L-I	Tuff
Calabash	10/29/69	22:01:51.43	5.7	L-I	Tuff
Halfbeak	06/30/66	22:15:00.07	6.0	300	Rhyolite (Pahute Mesa)

** Springer and Kinnaman (1971, 1975): L denotes 0 to 20
kt, L-I denotes 20 to 200 kt.

TABLE 5
EARTHQUAKE SAMPLE

<u>Date</u>	<u>Origin Time (UT)</u>	<u>Location</u>		<u>m_b</u>	<u>Focal Depth, km</u>
		<u>Latitude</u>	<u>Longitude</u>		
02/15/73	23:06:08.9	36.81N	115.90W	-	4
02/15/73	23:14:57.1	36.81N	115.91W	-	4
02/19/73	11:39:00.4	36.82N	115.92W	-	6
02/19/73	13:43:19.0	36.81N	115.88W	-	4
02/19/73	18:53:02.0	36.80N	115.81W	-	15
08/05/71	22:20:03.0	36.89N	115.94W	3.3*	9
01/24/72	13:30:53.9	36.71N	115.47W	3.4*	10
07/30/73	09:18:42.1	37.61N	115.15W	3.5*	5
12/06/67	01:33:04.6	37.10N	115.20W	3.7	33
08/05/71	20:46:36.7	36.90N	115.96W	3.9	4
05/17/68	14:11:20.0	37.63N	116.38W	4.0	15
04/06/66	17:56:32.1	37.20N	115.40W	4.1	33
08/10/70	10:48:56.4	37.19N	115.87W	4.1	3
02/09/73	23:10:34.4	36.84N	115.94W	4.2*	5
06/24/73	11:37:32.8	37.75N	116.15W	4.2	5
03/23/70	19:52:10.7	37.71N	115.99W	4.3	5
08/05/71	17:58:17.1	36.89N	115.97W	4.3	4
02/19/73	11:15:21.7	36.81N	115.92W	4.3	6
06/11/74	12:40:40.9	37.66N	115.29W	4.4	18
03/07/67	18:01:36.1	37.00N	115.00W	4.7	20

* M_s , m_b not available

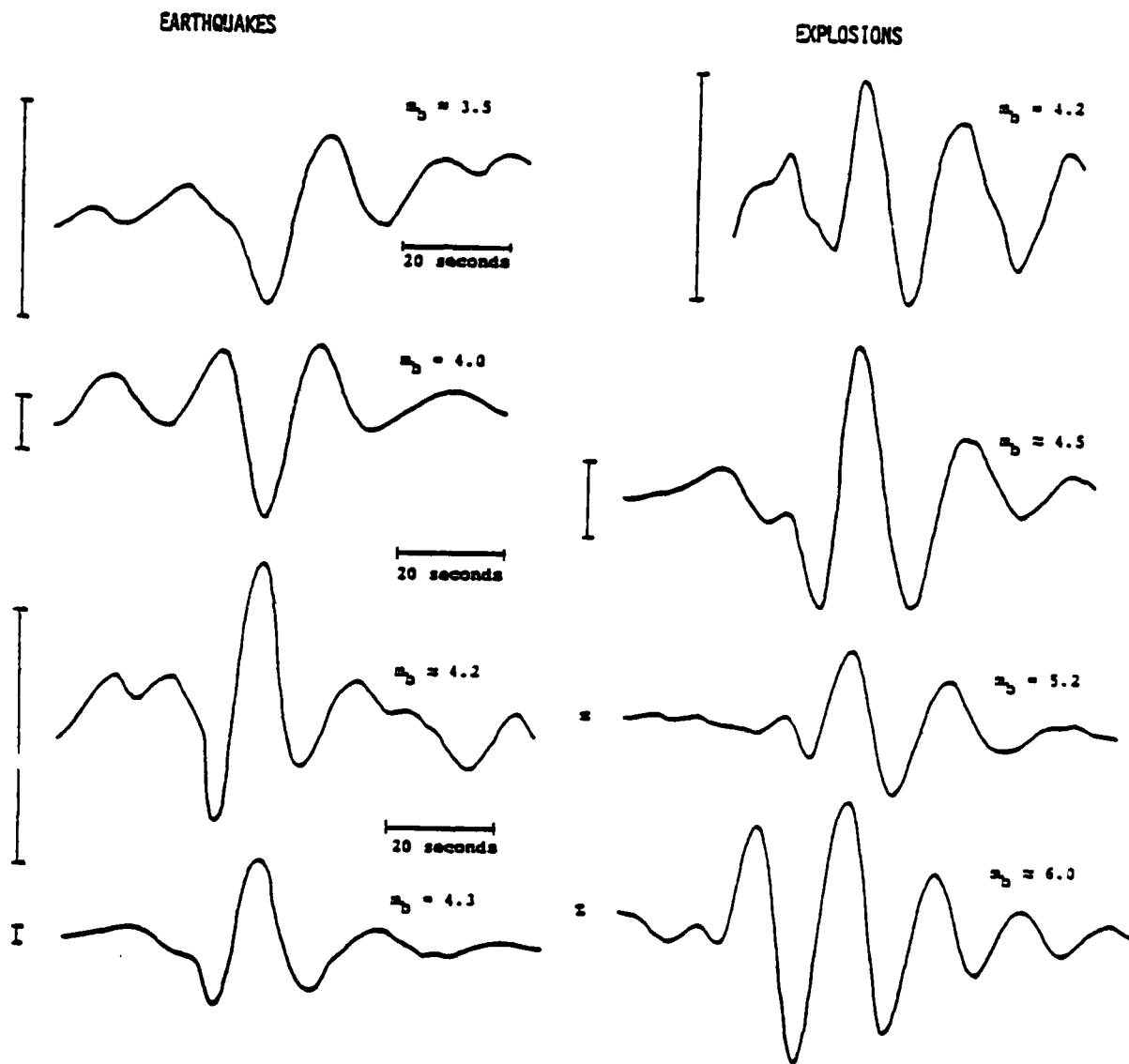


Figure 21. Typical long-period Rayleigh wave signals from NTS explosions and nearby earthquakes recorded at TFO. Vertical bars indicate relative amplitude scale.

In general, signals over the entire magnitude range for which we made measurements were clearly identifiable and consisted of rather simple, pulse-like waveforms similar to those shown. This characteristic of a consistent, simple signal over several orders of magnitude suggests the potential value of this phase for even small events where waveform filtering techniques could be used to extract the signal from background noise. Figure 22 displays the dominant period of the long-period Rayleigh wave signals for the events measured from the film records as a function of magnitude. Except for an apparent tendency for the explosion periods to be more consistent, there appears to be little evidence in the data of distinction between the dominant periods for earthquakes and explosions or as a function of magnitude. The data are generally intermingled, scattering between periods of 14 and 24 seconds and averaging 17 to 18 seconds. It should be noted that these periods are somewhat longer than those reported by previous investigators (e.g. Peppin and McEvelly (1974) and Bache et al. (1978) report dominant periods near 12 seconds and smaller). This difference is apparently attributable to differences in the responses of the seismograph systems involved. The TFO long-period response is peaked near 30 seconds and rolls off fairly rapidly at shorter periods.

With regard to use of amplitudes of the recorded phases to discriminate between earthquakes and explosions, our study has focused on comparison of amplitudes of the long-period Rayleigh wave signals and those of various short-period regional phases. Observations of discriminants based on the short-period regional phases alone recorded at TFO were reported in our previous annual report (Bennett et al., 1981) and were summarized above in the discussion of spectral discriminants. In brief, the principal characteristics of the short-period phases relevant to the current investigation can be summarized as follows: P_n phases recorded at TFO had low

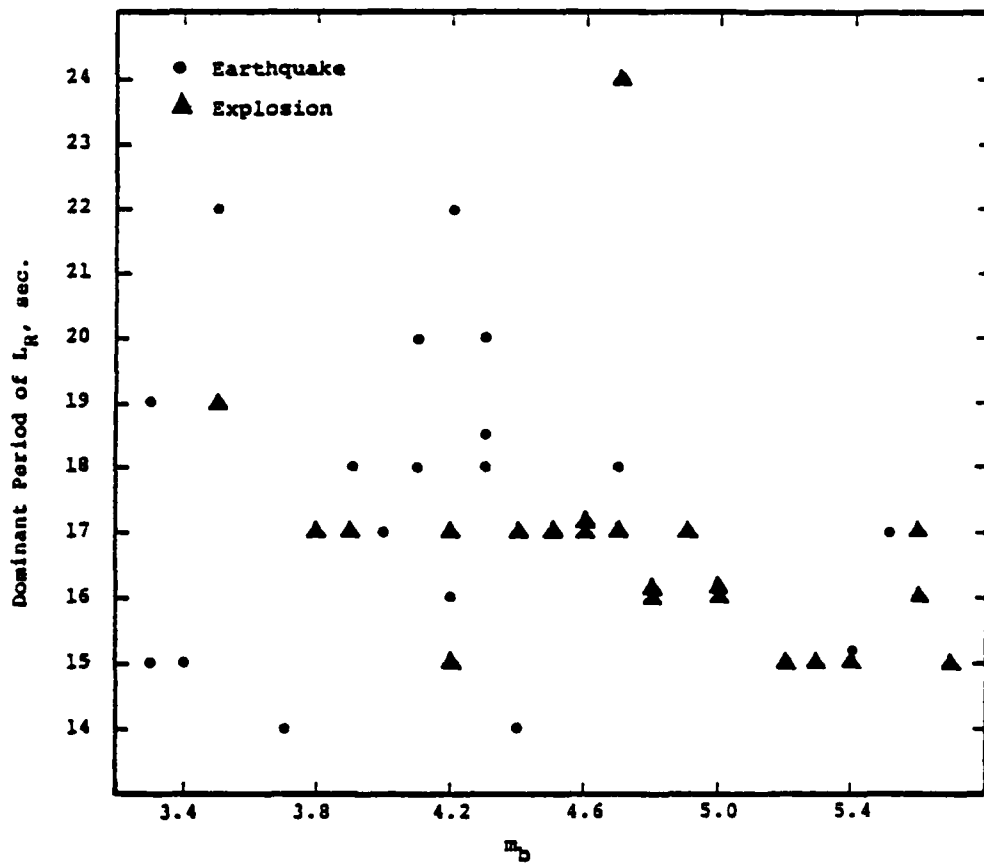


Figure 22. Dominant period of long-period Rayleigh wave pulses observed at TFO for NTS explosions and earthquakes as a function of network average m_b .

signal-to-noise ratios particularly for earthquakes (cf. Figures 2 and 3 above); but the P_g and L_g phases were generally strong (large signal-to-noise ratios), although nondiscrete, arrivals represented by prolonged wave trains raises some doubt regarding the significance of using maximum amplitudes to characterize these phases. Because of the nondiscrete nature of the short-period phases, identification of measured arrivals was generally based on group velocity windows.

The maximum amplitudes of all phases (long- and short-period) were measured from the film corresponding to the appropriate vertical instrument (in general, instrument location was constant) and converted to ground motion by dividing by the seismograph system gain at periods of 1 second and 20 seconds for the short- and long-periods respectively. More sophisticated corrections to adjust the amplitudes for the system response at the dominant period of the measured phase generally increased the scatter in the observation and, therefore, were not used.

Figure 23 shows the measured long-period Rayleigh wave amplitudes, L_R , in micrometers (μ) as a function of the reported body-wave magnitudes. Clearly, for a given m_b the earthquakes tend to generate larger long-period Rayleigh wave amplitudes than the corresponding explosions. This is demonstrated by the least squares trends shown by the straight lines in the figure. However, the scatter in the data points is large; and, in fact, several earthquake points appear to be scattered down into the explosion set at magnitudes near 4.

Figures 24, 25 and 26 show comparisons of the long-period Rayleigh-wave amplitudes with those of short-period regional phases P_n , P_g and L_g respectively, as measured at TFO. It should be noted that the number of data points in the different plots vary primarily due to variations in detection capability for the different phases over the limited dynamic range of the system; thus, the P_n phases may go un-

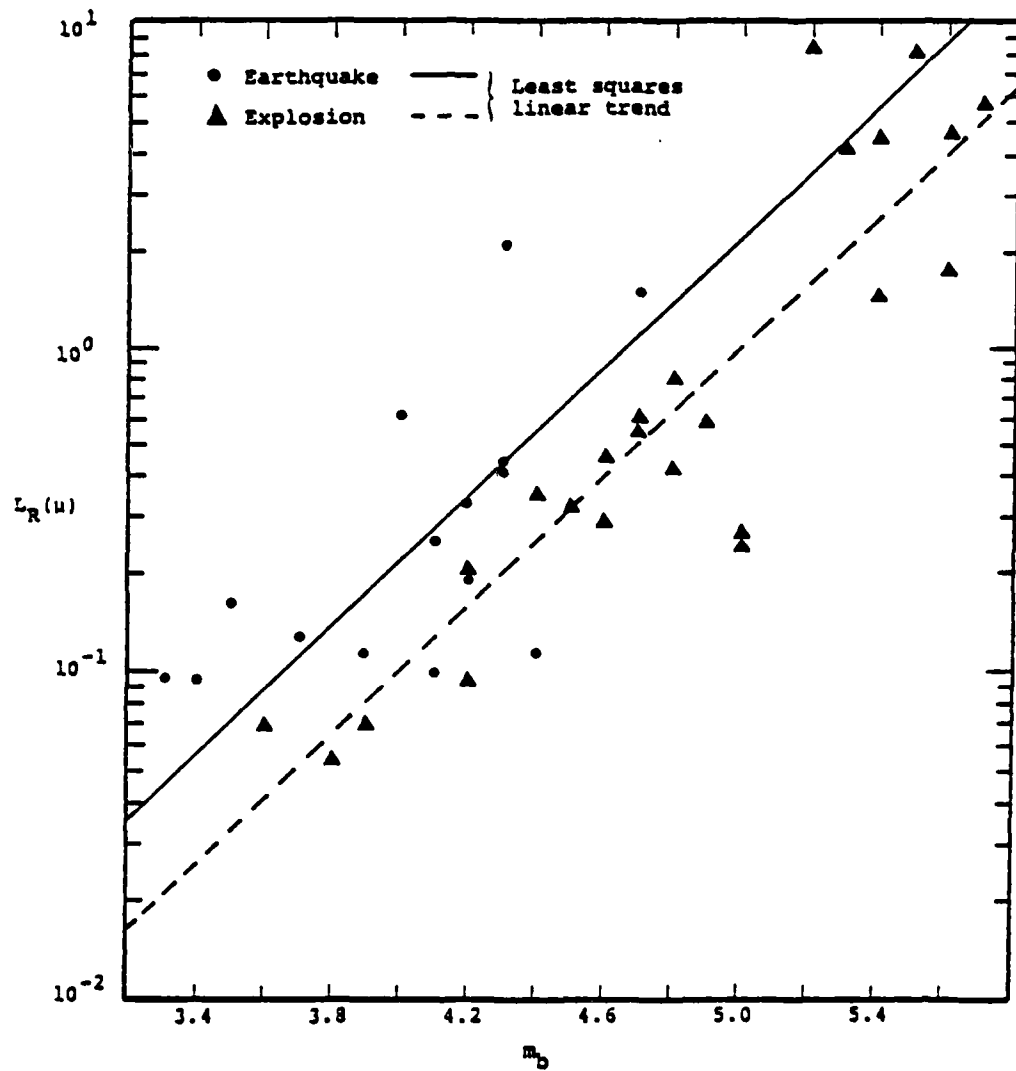


Figure 23. Amplitudes of long-period Rayleigh wave pulses observed at TFO for NTS explosions and earthquakes as a function of network average m_b . Slopes of the least-squares trends were constrained to one.

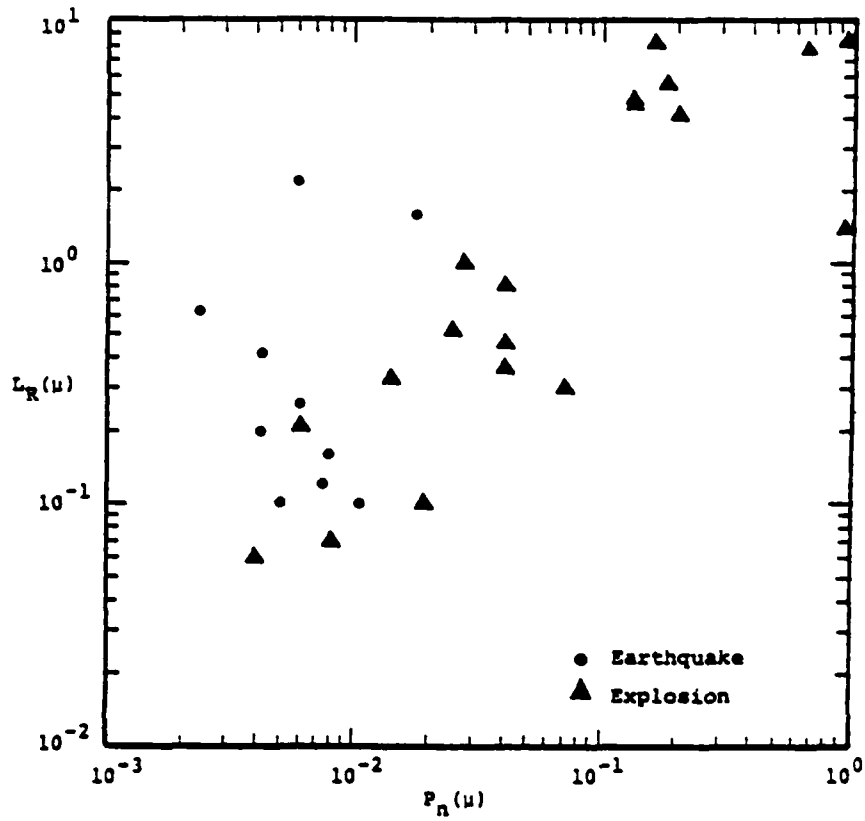


Figure 24. Amplitudes of long-period Rayleigh wave pulses versus short-period P_n for NTS explosions and earthquakes.

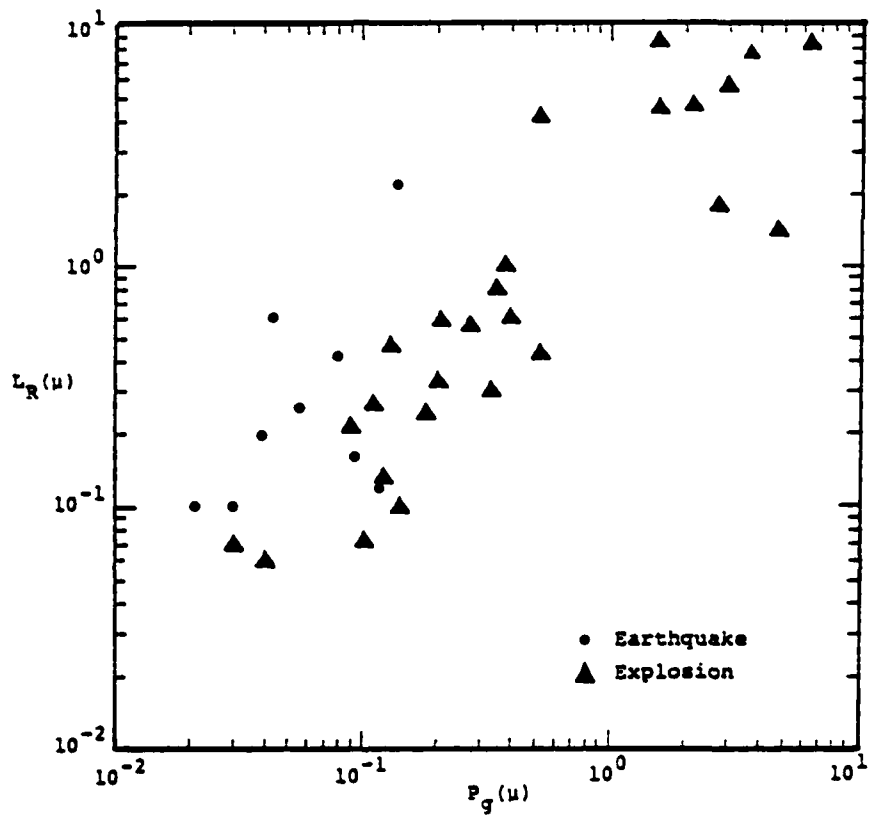


Figure 25. Amplitudes of long-period Rayleigh wave pulses versus short-period P_g for NTS explosions and earthquakes.

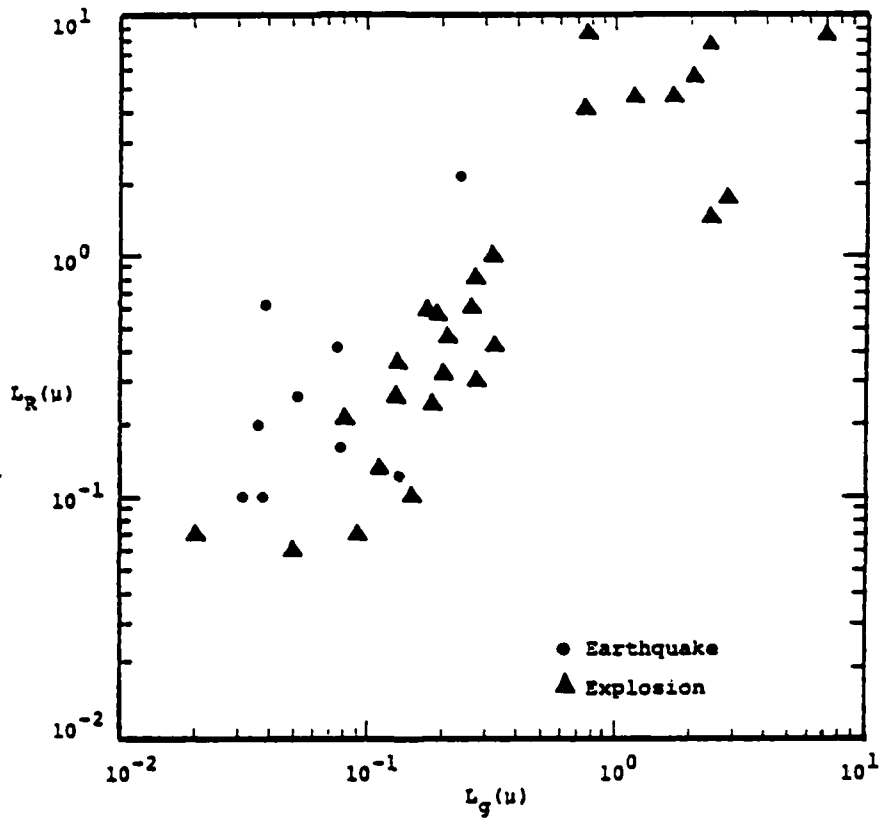


Figure 26. Amplitudes of long-period Rayleigh wave pulses versus short-period L_g for NTS explosions and earthquakes.

detected for small events while somewhat larger events produce P_g and/or L_g records which are off-scale. In the L_R versus P_n plot (Figure 24) the scatter in the data points is clearly worse than was seen in Figure 23 or than that found by Peppin and McEvilly (1974). The situation is particularly bad for the earthquake data which no longer show any kind of trend relating L_R and P_n . The most obvious cause of the observed deterioration is the attempt to measure P_n amplitudes in low S/N situations resulting in overestimates of P_n amplitudes. The low S/N of the P_n for the earthquakes was commented on above and is apparent in Figure 3.

Since the P_g and L_g amplitudes were generally stronger, we would expect less scatter in the L_R vs. P_g and L_R vs. L_g plots. Indeed, this appears to be the situation as can be seen in Figures 25 and 26. Here trends relating long- and short-period amplitude levels appear to be reestablished, and excitation of L_R for a given short-period regional phase amplitude is on the average larger for earthquakes than explosions. However, as was the case for the L_R vs. m_b plot noted above, some earthquake data points at the lower amplitude level appear to be scattered down into or intermingled with the explosion points. Such scatter does not appear to be attributable to noise contamination in the short-period measurements since the amplitudes of the downscattered earthquake points are generally larger than those of other points which do discriminate and are more than an order of magnitude larger than the P_n measurements which did appear to be affected by noise. A more likely explanation would seem to be that L_R measurements corresponding to the downscattered points were made nearer nodes in the long-period radiation pattern although this argument is speculative at this time since the focal mechanisms are unknown. An alternate possibility explaining the lack of separation is that the L_R amplitudes are overestimated for the explosions. The reasonableness of the observed long-period Rayleigh wave amplitudes

from the explosion sources will be discussed in more detail below.

To better understand the properties of the long-period Rayleigh wave signal and to test the validity of its observed characteristics, theoretical seismograms were computed. A conventional Harkrider model (Harkrider 1964, 1970) for an explosion source in a horizontally layered earth was used. The explosion was assumed to be buried at a depth of 500 m in a crustal model representative of Yucca Flat (cf. Figure 27). The generated motions were assumed to propagate between the source and receiver in a crustal model developed for this region in an independent study by Bache et al. (1978) of long-period Rayleigh wave dispersion for the path from NTS to Tucson. This propagation model is shown in Figure 27. Coupling of energy between the source crust and transmission crust was achieved using a method described by Alewine (1974) and Bache et al. (1978) which assumes constant horizontal energy flux with no mode conversions or refraction effects at the boundary between the two crustal models. Within the transmission path crustal model, motions were allowed to attenuate by letting Q_2 be 300 in the upper half of the crust, 1000 in the lower half and 150 in the mantle. The computed vertical ground motions were then convolved with the instrument response of the TFO long-period seismograph system to obtain the synthetic time history shown in Figure 27. For purpose of comparison an actual long-period Rayleigh wave signal from a magnitude 4.5 (m_p) explosion is shown at the bottom of the figure; in this case the synthetic has been arbitrarily scaled to an amplitude similar to that of the explosion. The characteristics of the observed and synthetic seismograms are remarkably similar. The simple pulse-like character of the synthetic signal closely matches the observations, and the dominant periods are nearly the same.

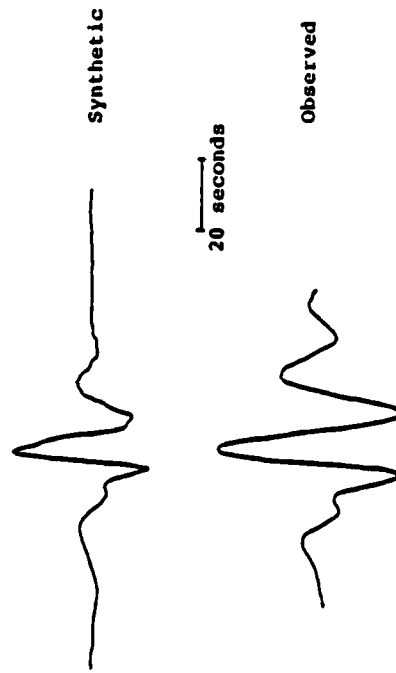
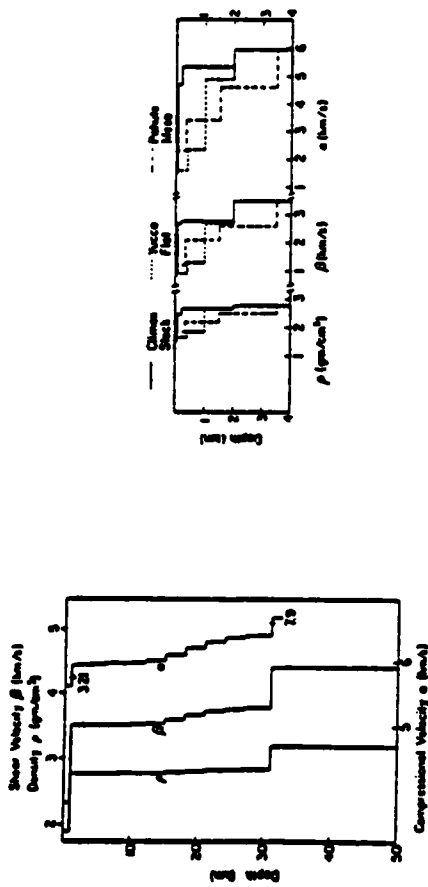


Figure 27. Transmission path crustal model (top left) and source crustal model (top right) used to compute synthetic seismogram (middle) for an NTS explosion recorded on long-period seismograph at TFO as compared with an observed signal (bottom).

With regard to amplitudes, we used standard scaling equations (cf. Mueller and Murphy, 1971) to derive a relation between the amplitude of the synthetic seismogram (predicted amplitude) and the yield. In brief, the scaling goes as follows: The amplitude of the long-period Rayleigh wave is taken to be directly proportional to the steady-state reduced displacement potential (RDP)

$$\frac{A_1}{A_0} = \frac{\psi_1(\infty)}{\psi_0(\infty)}$$

where the A's are amplitudes at some fixed recording station corresponding to the RDP levels, $\psi(\infty)$, associated with contained explosion sources in a common source medium. The RDP is related to the radius of the cavity created by the explosion, r_c , as

$$\psi(\infty) = k_1 r_c^3/3$$

where k_1 is a medium-dependent constant which is usually taken as equal to 1.0 for granite and 0.6 for tuff and alluvium. The cavity radius is further related to yield, W, in kilotons and depth of burial, h, in meters according to

$$r_c = k_2 W^{0.29}/h^{0.11}$$

where k_2 is again dependent on the emplacement medium and is estimated as 24.66 for granite, 31.41 for tuff and 28.70 for alluvium. Combining these we obtain:

$$\psi(\infty) = \frac{k_1}{3k_2} \frac{W^{0.87}}{h^{0.33}}$$

If we have an independent measure of the yield and depth of burial for some explosion, we can then calculate the associated RDP. If A_0 is the computed amplitude corresponding to the

synthetic seismogram generated by the explosive source with an associated RDP, $\psi_0(\infty)$, then Rayleigh wave amplitudes, A_1 , for events with other RDP's, $\psi_1(\infty)$, can be calculated using the above relationships.

Figure 28 shows a comparison of amplitudes measured at TFO with amplitudes predicted on the basis of the scaling relationships and using teleseismic yield estimates from Dahlman and Israelson (1977). Circled events are from Yucca Flat, uncircled tuff events are from Pahute and Rainier Mesas, the granite event was at Climax Stock and the rhyolite event was at Pahute Mesa. The straight line corresponds to the condition where the prediction matches the observation. Thus, the observed amplitudes seem to be in reasonable agreement with the predicted values; if anything, the predicted values are generally somewhat large.* A possible physical explanation of large predicted amplitudes for the Yucca Flat events would be compaction in the dry alluvium and tuff source materials which is not completely accounted for in the scaling models. The resulting overestimate of the RDP's associated with the radiated seismic energy would cause the anomalous predicted values. On the other hand, disregarding this physical explanation for the moment, the agreement between the predicted and observed amplitudes suggests that the observed intermingling of the earthquake and explosion data is real. In fact, if the somewhat larger predicted values of L_R were substituted for the observed, they would tend to increase the intermingling.

* It should be noted that, in estimating the transmission coefficient for the transition from source to transmission crust, no account was taken of NTS source regions other than Yucca Flat. A more complete consideration of this factor would cause the granite observation (Piledriver) to be shifted nearer the predicted value and shift other predictions for events not on Yucca Flat to slightly higher values.

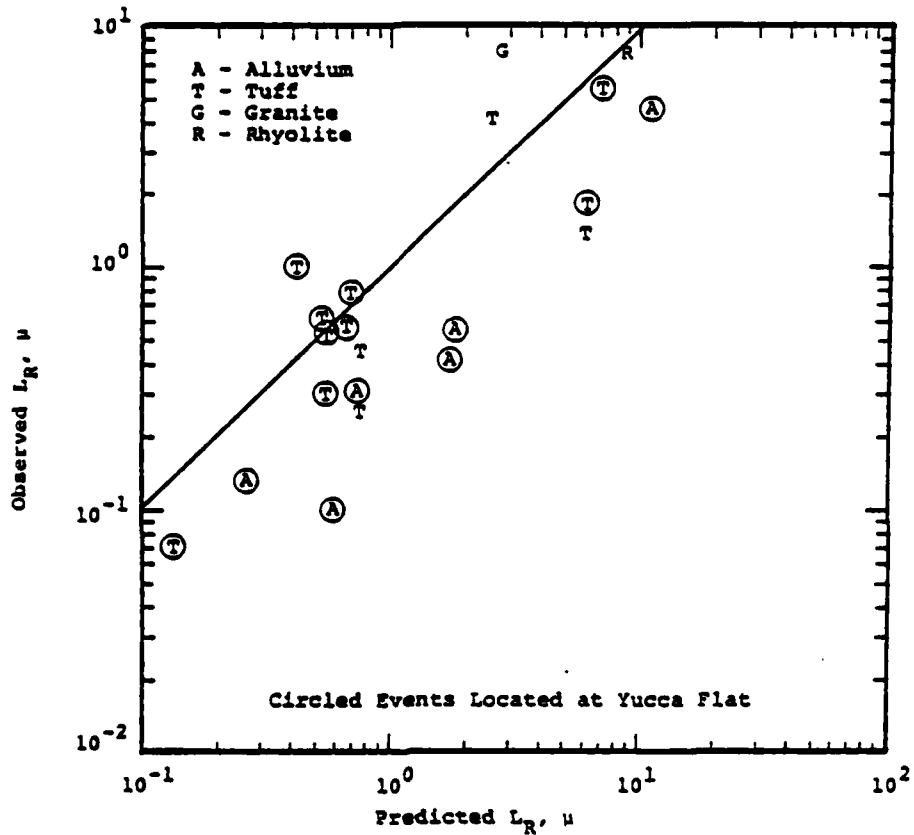


Figure 28. Comparison of observed and predicted long-period Rayleigh wave amplitudes for NTS explosions in various source media. Straight line corresponds to observed amplitude equal to that predicted using standard scaling relations and teleseismic yield estimate.

IV. SUMMARY AND CONCLUSIONS

4.1 SUMMARY

The investigations summarized in this report have centered on an attempt to assess the discrimination potential associated with regional seismic phases using data recorded at the Tonto Forest Observatory (TFO) in Arizona from Nevada Test Site (NTS) explosions and nearby earthquakes. This effort has encompassed comparative studies of the spectral composition of the regional phases P_n , P_g and L_g recorded from the two source types as well as an assessment of the applicability of long-period regional data to the discrimination of small events for which teleseismic M_s values cannot be determined.

A detailed analysis of the characteristics of the short-period regional phase data observed at TFO from NTS explosions and nearby earthquakes was presented in Section II, where spectra were derived for a large sample of events and used to characterize the average frequency content of the P_n , P_g and L_g phases generated by the two source types. Using these data, it was demonstrated that while the average spectral shapes of the P_n and P_g phases from the two source types do not show statistically significant differences, the average earthquake L_g phase appears to be significantly richer in high frequency content than the corresponding average explosion L_g phase having the same maximum spectral amplitude level. On the basis of this observation, a preliminary L_g spectral ratio discriminant was defined and applied to the available data set and shown to provide almost complete separation of the data from the two source types. Finally, some preliminary theoretical simulations of earthquake and explosion L_g spectra were described and shown to be inconsistent with the observed differences in L_g spectral composition.

The current status of the investigation into the utility of long-period regional data for seismic discrimina-

tion purposes was summarized in Section III. This portion of the study focused on a time-domain analysis of long-period Rayleigh wave data recorded at TFO from a sample of NTS explosions and nearby earthquakes. The observed maximum amplitudes of these long-period phases were plotted against both the maximum amplitudes of the corresponding P_n , P_g and L_g phases and the associated teleseismic m_b values to provide regional analogs of the M_s/m_b discriminant. Although it was found that, on the average, these single station displays separate the data from the two source types, it was demonstrated that they are not particularly reliable for small events with m_b values less than about 4.0.

4.2 CONCLUSIONS

The analyses described above support the following conclusions concerning the characteristics of the short-period regional phase data recorded at TFO from NTS explosions and nearby earthquakes.

1. Although the observed L_g phases from earthquakes are typically more prominent than those from explosions with comparable P wave amplitude levels, simple time-domain L_g/P amplitude ratios do not provide a consistent separation of the data from the two source types.
2. The spectral composition of the P_n and P_g phases recorded from earthquakes and explosions of the same body wave magnitude are not significantly different over the usable frequency band extending from about 0.5 to 5.0 Hz. However, the earthquake L_g spectra are found to be significantly richer in high frequency content than corresponding explosion spectra having the same maximum spectral amplitude level.

3. An L_g spectral discriminant defined as the ratio of the average spectral amplitude level in the 0.5 to 1.0 Hz passband to the average spectral amplitude level in the 2.0 to 4.0 Hz passband was found to provide good separation between the earthquake and explosion populations over the magnitude range $3.3 \leq m_b \leq 4.8$. The average separation was found to be about a factor of three, independent of the component of motion employed.
4. Comparable diagnostic differences have been noted in the spectral composition of the L_g phases recorded from the Eastern U.S. Salmon explosion and the nearby Alabama earthquake of 2/8/64. This suggests that the observed L_g spectral differences are not due to any peculiarities in the NTS to TFO propagation path or to unusual source characteristics of Yucca Flat explosions in alluvium and tuff.
5. Preliminary theoretical simulations of the L_g spectra to be expected from explosions and earthquakes have failed to provide any quantitative insight into why the L_g spectral discriminant works. It appears that more sophisticated theoretical models will be required to match the important characteristics of the observed spectra.

With regard to the long-period regional data, results of studies conducted to date lead to the following conclusions.

1. Long-period Rayleigh waves recorded at TFO from NTS explosions and nearby earthquakes are characterized by simple, pulse-like arrivals with

dominant periods averaging 17 to 18 seconds and are observable from events with body wave magnitudes as low as 3.3.

2. For a fixed teleseismic m_b value, or fixed maximum amplitude of an associated short-period phase (i.e. P_n , P_g , L_g), observed maximum Rayleigh wave amplitudes are typically larger for earthquakes than for explosions. However, below about $m_b = 4.0$, there is considerable scatter in the data and intermingling of the earthquake and explosion populations. This suggests that single station M_s/m_b type discriminants may not be effective against small events, even if regional data are available.
3. The explosion Rayleigh wave data observed at TFO can be simulated with good accuracy using simple models of the explosion source and Rayleigh wave propagation effects. On the basis of these simulations it has been concluded that the observed Rayleigh wave amplitudes at TFO are reasonably consistent with the static values of the reduced displacement potential ($\psi(\infty)$) which would be predicted using the expected final cavity radii for these events.

REFERENCES

- Alewine, R. W. (1974), "Application of Linear Inversion Theory Toward the Estimation of Seismic Source Parameters," Ph.D. Thesis, California Institute of Technology.
- Bache, T. C., W. L. Rodi and D. G. Harkrider (1978), "Crustal Structures Inferred from Rayleigh-Wave Signatures of NTS Explosions," BSSA, 68, pp. 1399-1413.
- Bache, T. C., H. J. Swanger, B. Shkoller and S. M. Day (1981), "Simulation of Short Period L_g , Expansion of Three-Dimensional Source Simulation Capabilities and Simulation of Near-Field Ground Motion From the 1971 San Fernando, California, Earthquake," SSS-R-81-4668, September.
- Bakun, W. H. and L. R. Johnson (1971), "Short Period Spectral Discriminants for Explosions," Geophys. J., 22, pp. 139-152.
- Bennett, T. J., D. G. Lambert, J. R. Murphy, J. M. Savino and C. B. Archambeau (1981), "Regional Discrimination Research," SSS-R-81-5032, June.
- Blandford, R. R. (1981), "Seismic Discrimination Problems at Regional Distances" in Identification of Seismic Sources - Earthquake or Underground Explosions, D. Reidel Publishing Company, Boston.
- Fisher, F. G., P. J. Papanek and R. M. Hamilton (1972), "The Massachusetts Mountain Earthquake of 5 August 1971 and its Aftershocks, Nevada Test Site," U.S.G.S. Paper 474-149.
- Gupta, I. and R. Blandford (1981), "A Mechanism for Generation of Short-Period Transverse Motion from Explosions" presented at VSC Research Conference, November, 1981.

REFERENCES (Cont'd)

- Harkrider, D. G. (1964), "Surface Waves in Multilayered Media I. Rayleigh and Love Waves from Buried Sources in Multilayered Elastic Half-Space," BSSA, 54, pp. 627-672.
- Harkrider, D. G. (1970), "Surface Waves in Multilayered Media II. Higher Mode Spectra and Spectral Ratios from Point Sources in Plane-Layered Earth Models," BSSA, 60, pp. 1937-1987.
- Lambert, D. G. and S. S. Alexander (1971), "Relationships of Body and Surface Wave Magnitudes for Small Earthquakes and Explosions," Teledyne Geotech Report.
- Mueller, R. A. and J. R. Murphy (1971), "Seismic Characteristics of Underground Nuclear Detonations: Part I. Seismic Spectrum Scaling," BSSA, 61, pp. 1675-1692.
- Murphy, J. R. (1975), "Analysis of Near-Field Ground Motion Spectra From Earthquakes and Explosions," Semi-Annual Technical Report to Advanced Research Projects Agency, Computer Sciences Corporation, February.
- Peppin, W. A. and T. V. McEvelly (1974), "Discrimination among Small Magnitude Events on Nevada Test Site," Geophys. J., 37, pp. 227-243.
- Peppin, W. A. (1976), "P-Wave Spectra of Nevada Test Site Events at Near and Very Near Distances: Implications for a Near-Regional Body Wave-Surface Wave Discriminant," BSSA, 66, pp. 803-825.
- Pomeroy, P. (1980), "Regional Seismic Wave Propagation," Rondout Associates Final Technical Report, Air Force Office of Scientific Research Contract F49620-78-C-0043.
- Priestly, K. and J. Brune (1978), "Surface Waves and the Structure of the Great Basin of Nevada and Western Utah," JGR, 83, pp. 2265-2272.

REFERENCES (Cont'd)

Springer, D. L. and R. L. Kinnaman (1971), "Seismic Source Summary for U.S. Underground Nuclear Explosions, 1961-1970," BSSA, 61, pp. 1073-1098.

Springer, D. L. and R. L. Kinnaman (1975), "Seismic Source Summary for U.S. Underground Nuclear Explosions, 1971-1973," BSSA, 65, pp. 343-349.

Willis, D. E., J. DeNoyer and J. T. Wilson (1963), "Differentiation of Earthquakes and Underground Nuclear Explosions on the Basis of Amplitude Characteristics," BSSA, 53, pp. 979-987.